Shear Strengthening of Reinforced Concrete Beams with Hybrid Composite Plates

Hadi Baghi[1,*], Joaquim A. O. Barros[1] and António Ventura-Gouveia [2]

[1] ISISE, Department of Civil Engineering, University of Minho, Guimarães, Portugal

[2] ISISE, Department of Civil Engineering, School of Technology and Management of Viseu, Viseu, Portugal

Abstract:

The effectiveness of Hybrid Composite Plates (HCPs) for the shear strengthening of the Reinforced Concrete (RC) beams was assessed by an experimental program. HCP is a thin plate of Strain Hardening Cementitious Composite (SHCC) reinforced with Carbon Fiber Reinforced Polymer (CFRP) laminates. Due to the excellent bond conditions between SHCC and CFRP laminates, these reinforcements provide the necessary tensile strength capacity to the HCP. Two HCPs with different inclination of CFRP laminates (45º and 90º) were adopted for the shear strengthening of RC beams by bonding these HCPs to the lateral faces of the beam with an epoxy adhesive. The results showed that these HCPs have assured a significant increase in terms of load carrying capacity, mainly those with inclined laminates. The SHCC surrounding the CFRP laminates in the HCP has offered effective resistance to the degeneration of micro-cracks on macro-cracks, which has avoided the occurrence of premature mixed shallow-semi-pyramid-plus-debonding failure modes registered currently when using the NSM-CFRP technique. Advanced numerical simulations were performed by using a FEM-based computer program, whose predictive performance was demonstrated by simulating the experimental tests carried out. In this context a parametric study was executed to evaluate the shear strengthening efficiency of the arrangement and percentage of CFRP laminates in HCPs, as well as the influence of using mechanical anchors to avoid premature detachment of the HCPs.

Key words: Strain Hardening Cement Composites, Near Surface Mounted, CFRP laminates, Shear strengthening of reinforced concrete beams, Numerical simulation, Finite Element Method.

* Corresponding author. Email address: hadibaghi@gmail.com; Fax: +351-253-510-217; Tel: +351-918-491-472.

Introduction:

There is a great need for upgrading Reinforced Concrete (RC) structures all over the world to carry higher ultimate loads or to satisfy certain serviceability requirements. One of the strengthening methods that have been applied in the last three decades includes the external bonding of thin steel plates to tensile or shear regions of the RC members using an epoxy adhesive or mechanical anchors (Su *et al.* 2010). However, there are two major disadvantages of this method: difficulty to manipulate the steel plates at the construction site due to their weight, and also durability weakness associated with a reduction in the bond between steel plates surface and adhesive, or even the susceptibility of the steel plates to corrosion (Abdel-Jaber *et al.* 2003; Saafan 2006).

Fiber reinforced polymer (FRP) composite materials are regarded as an alternative for externally bonded steel plates, by adopting externally bonded reinforcement (EBR) technique. Numerous research studies have been carried out to evaluate the efficiency of the EBR technique to increase the flexural and shear strength of RC members (Khalifa *et al.* 1998; Abdel-Jaber *et al.* 2003). However, this technique has some issues that can compromise its strengthening effectiveness such as: debonding of the FRP, lack of protection (vandalism and fire), preparation of the surface, and stress concentration caused by anchorage devices when used for avoiding the premature debonding of the FRP (Chaallal *et al.* 2011).

The Near Surface Mounted (NSM) FRP laminates/rods is another strengthening technique that has been used to increase the shear capacity of RC beams. In this method, carbon fiber reinforced polymer (CFRP) laminates/rods are embedded into grooves open on the concrete cover using an adhesive. Research has shown that a significant increase in the shear resistance of RC beams is reachable using the NSM CFRP technique (Lorenzis and Nanni 2001; Dias and Barros 2010; Rezazadeh *et al.* 2014). However, debonding of the FRP laminates/rods and/or fracture of concrete surrounding these composites are still inevitable, and limiting their strengthening potential (Bianco *et al.* 2011; Dias and Barros 2013).

Strain Hardening Cementitious Composite (SHCC) is a class of fiber reinforced cement composites (FRCC) that exhibits ductile behavior under tensile load, with a strain hardening response rather than the tension softening character presented by conventional FRCC after crack initiation (Li 1998). In SHCC materials, the fiber bridging mechanisms developed during the crack opening process allow a gradual increase of tensile capacity from crack initiation up to a relatively high tensile strain (more than 1%), where a failure macro-crack finally occurs, followed by a strain-softening stage. The tensile strain hardening phase is accompanied by the formation of a diffuse crack

2

pattern of very small crack width. In recent years, SHCC has been used for developing new construction systems and for the structural rehabilitation since this type of materials exhibits ductile shear response (Shang and Zijl 2007), high energy absorption capacity, and stable hysteretic loops even at large drifts (Parra-Montesinos and Wight 2000). Recently it was demonstrated the potentialities of using prefabricated SHCC plates reinforced with CFRP sheets for the shear strengthening of deep beams (Esmaeeli *et al.* 2013a). This concept was extended to the use of CFRP laminates applied according to the NSM technique, and also explored the use of chemical anchors for assuring better fixing conditions for these Hybrid Composite Plates (HCPs). These HCPs were capable of restoring, and even increase, the hysteretic response, energy dissipation, and also the load carrying capacity of beam-column joint that were previously damaged (Esmaeeli *et al.* 2015). HCPs were also very efficient for the increase of the flexural capacity of RC beams (Esmaeeli *et al.* 2014). Besides the contribution of the SHCC for the strengthening efficiency of HCPs, the SHCC also assures some protection to the CFRP laminates and adhesive such as vandalism, aggressive environmental conditions, and fire. The combination of SHCC and CFRP grids was also explored in the context of the development of innovative hybrid composite system for the structural rehabilitation, where the benefits of combining these materials in terms of load carrying capacity, ductility and cracking behavior were demonstrated by Orosz *et al.* (2013).

In this present work, the effectiveness of HCPs to increase the shear resistance of RC beams is assessed. For this purpose an experimental program of six rectangular cross section RC beams was carried out, composed of two control beams and four beams strengthened in shear, one with NSM-CFRP laminates, another one with SHCC plates, and the others two with HCPs where the unique difference is the inclination of the laminates (45º, and 90º). For better understanding of the effectiveness of this technique an advance numerical simulation was carried out. By using the properties obtained from the experimental program for the characterization of the relevant properties of the used materials, the data for defining the crack shear softening diagram of the adopted multi-fixed smeared crack constitutive model was derived from inverse analysis by simulating the beams tested experimentally. These simulations have fitted with high accuracy the deformational response and the crack pattern of the tested beams. Thus a parametric study was carried out for assessing the influence, on the shear strengthening effectiveness of RC beams, of the strengthening configuration and percentage of CFRP laminates in HCPs, as well as the use of mechanical anchors to prevent detachment of the HCPs.

1   **Experimental Program:**

2   *Series of Beams:*

3   The beams of the experimental program have a rectangular cross section (150mm×300mm) with the length of

4   2500mm, and 2200mm clear span (Figure 1). The longitudinal steel reinforcement consisted of 2ϕ20 laid at the

5   bottom and 2ϕ10 at the top as tensile and compression reinforcement, respectively, giving to the beam's cross

6   section an effective depth (d) of 261mm. The steel bars were anchored at the section of the supports with 90°

7   hooks to prevent premature anchorage failure and sliding. To localize the shear failure in only one of the shear

8   spans, a three point bending test setup with different length of the shear spans was selected, as shown in Figure 1.

9   Since the monitored shear span (L_i) has a length of 800mm, a shear span to effective depth ratio (L_i / d) of 3 was

10   assured for minimizing the arching effect (Dias and Barros 2010). A relatively high percentage of steel stirrups

11   (ϕ8@100 mm) was applied in the other span (L_r) to avoid that shear failure occurs in this span. Depending on the

12   number of the steel stirrups in the L_i, the beams were categorized in two different types. The type A was designed

13   with steel stirrups ϕ8@100mm, while type B did not include any transverse reinforcement in this span in an attempt

14   of assuring flexural and shear failure mode for these respective beams. Four beams of type B were strengthened in

15   shear with the following three different techniques: 1) NSM-CFRP laminates; 2) SHCC plates; and 3) HCPs with

16   two inclinations of the CFRP laminate (45º and 90º).

17   This experimental program aims to compare the effectiveness of these shear strengthening techniques, as well as the

18   influence of the inclination of the CFRP laminates in the HCPs for the shear strengthening of RC beams.

19   The characteristics of the beams are presented in Table 1. The 7S-R beam had 7 stirrups in L_i span in order to

20   assure flexural failure. The 0S-R was a control beam without any type of shear reinforcement and strengthening in

21   the L_i span. The NSM-4L90 beam was shear strengthened with four vertical CFRP laminates in each lateral face of

22   L_i span, spaced at 180 mm, and applied according to the NSM technique. The SP beam was strengthened with

23   SHCC plates applied in each lateral face of L_i span to investigate the effectiveness of these plates for the shear

24   strengthening. These plates had overall dimensions of 720×300×20 mm and were bonded to the concrete beam using

25   an epoxy adhesive (S&P220 supplied by Clever Reinforcement company). The SP-4L90 and SP-3L45 beams were

4

1   strengthened by applying HCPs in each lateral face of the L_i span. As shown in Figure 2(c), the HCP is a 20mm

2   thick SHCC plate that includes a strengthening system formed by CFRP laminates positioned at 45º (applied in SP-

3   3L45 beam) or 90º (applied in SP-4L90 beam).

4   The SHCC plates were cut from the panels with a size of 800×800×20 mm that were built, each one, with a batch of

5   about 13 liters of SHCC. After casting, these panels were sealed by a plastic sheet and were kept in a room

6   environment for 24 hours before de-molding. After de-molding, all these panels were transferred to the climate room

7   and were cured under the constant conditions of 20°C temperature and 80% humidity up to the age of 28 days, in

8   order to follow the curing procedure recommended in Esmaeeli *et al.* (2012) for these type of panels.

9   The NSM-4L90, SP-4L90, and SP-3L45 beams had equal percentage of CFRP laminates. The CFRP shear

10   strengthening percentage, ρ_{fw}, is obtained from:

$$\rho_{fw} = \frac{2a_f b_f}{b_w s_f \sin\theta_f} \tag{1}$$

11   where $b_w = 150$ mm is width of the beam's cross section, $a_f = 1.4$ mm and $b_f = 10$ mm are the dimensions of the

12   NSM CFRP laminate cross section, and s_f and θ_f represent the spacing and inclination of these laminates,

13   respectively (Figure 2).

14

15   *Test Setup and Monitoring System*

16   The load was applied by using a servo closed loop control equipment, taking the signal read in the displacement

17   transducer (LVDT) of the servo-actuator to control the test at a deflection rate of 0.01 mm/s. The deflections of the

18   beams at loaded section and at mid-span were measured by two LVDTs. These LVDTs were supported on an

19   aluminum bar fixed at the alignments of the supports of the beams (Figure 3(a)) in order to avoid readings support

20   settlements and deformability of the test reaction frame (Costa and Barros 2010). With the purpose of obtaining the

21   strain variation along the laminates, strain gauges (SG) were bonded to the CFRP laminates according to the

22   arrangement represented in Figure 3(b). A 50mm spaced grid was drawn on the L_i span of the beams in order to

23   have a reference system for recording the crack pattern by using a photo-camera.

24

25   *Material Properties*

The concrete compressive strength was evaluated at 28 days and at the age when the beam were tested (99 days) by executing direct compression tests with cylinders of 150mm diameter and 300mm height according to EN206-1 recommendation (European standard 2000). The values of tensile properties of the steel bars were obtained from uniaxial tensile tests executed according to EN10002-1 recommendations (European Standard 1990). The tensile properties of the CFRP laminates and epoxy adhesive were characterized by executing uniaxial tensile tests according to the recommendations of ISO 527-5 (European Standard 1997) and ISO 527-2 (European Standard 1996), respectively.

The SHCC is composed of a cementitious mortar reinforced with 2% of volume of short discrete polyvinyl alcohol (PVA) fibers. The SHCC mix was prepared based on a previous study (Esmaeeli *et al.* 2013b). The dry ingredient materials (sand, S, cement, C, and fly ash, FA) were firstly mixed. In the second step, the superplasticizer (SP) and a quarter of the water (W) were combined and added to the dry ingredient materials. The rest of the water and the viscous modifier agent (VMA) were then combined and introduced into the mix. Finally, PVA fibers were added to the mortar. The SHCC mix procedure and proportions are presented in Table 2 and Table 3, respectively (Esmaeeli *et al.* 2013b). The envelope and the average tensile stress versus crack opening displacement (COD) obtained in notched specimens are presented in Figure 4 (Esmaeeli *et al.* 2013b). According to these results, the average tensile stress at crack initiation and the average tensile strength of the SHCC were 2.7 and 3.5MPa, respectively. Table 4 represents the average values obtained from the experimental programs for the assessment of the relevant properties of the concrete, steel bars, CFRP laminates, adhesive epoxy, and SHCC.

Strengthening Techniques

Three different strengthening techniques were used in this project: i) NSM CFRP laminates, ii) SHCC plates, and iii) HCPs. The CFRP laminates were applied to the NSM-4L90 beam according to the NSM technique described in Dias and Barros (2013). The slits that were opened on the lateral faces of the RC beams for the installation of the CFRP laminates had a width and depth of 5 and 15 mm, respectively.

The CFRP laminates adopted for the reinforcement of the SHCC plates have followed a procedure similar to the one taken for the NSM-4L90 beam. However, in this case the slits on the SHCC plates had a width and a depth of about 4 and 11mm, respectively, spaced at 180 mm and 250 mm for the SP-4L90 ($\theta_f = 90°$) and SP-3L45 ($\theta_f = 45°$)

1 beams, respectively (Figure 2(a) and 2(b)). The HCPs were applied to their corresponding beams 5 days after the

2 application of the CFRP laminates in order to guarantee a proper curing of the adhesive.

3 To apply the SHCC plates and HCPs to the lateral faces of the concrete beams on L_i span, the following procedures

4 were executed: 1) a 1-2 mm roughness with sandblast was executed in each lateral face of L_i span to improve the

5 bond conditions between SHCC/HCPs and concrete beams (the inspection of the tested beams showed that no slip

6 occurred between substrate and SHCC/HCPs); 2) the surfaces of the beams were cleaned by compressed air; 3) an

7 epoxy adhesive (S&P220) layer of a thickness of about 1mm was homogenously applied in the surfaces of the

8 concrete beams and of the SHCC/HCPs that will be in contact; 4) mechanical clamps were used to maintain the

9 SHCC/HPCs pressed against the lateral surfaces of the beam up to the time that the epoxy resin developed its initial

10 bond. To guarantee a proper curing of the adhesive, one week passed between the beams strengthening operation

11 and the beam's test.

12

13 **Presentation and discussion of results**

14 *Global Analysis*

15 The load versus deflection curves of the tested beams are represented in Figure 5(a). The SP-4L90 and SP-3L45

16 beams presented higher load carrying capacity and stiffness than the other beams, except 7S-R beam, which reveals

17 the shear strengthening effectiveness of the HCPs for the overall behavior of this type of beams. The maximum load

18 and its corresponding deflection of the tested beams are included in Table 5. The maximum deflection at the loaded

19 section, at peak load, of the SP-3L45 beam was 1.5 and 2.0 times higher than the corresponding deflection of the

20 SP-4L90 and SP beams, respectively. From the obtained results the $\Delta F_{max} / F_{max}^{0S-R} = (F_{max} - F_{max}^{0S-R}) / F_{max}^{0S-R}$

21 ratio was evaluated, and the values are indicated in Table 5, where F_{max}^{0S-R} and F_{max} are the maximum load

22 capacity of the 0S-R beam and shear strengthened beams, respectively. For deflections greater than the

23 corresponding to the formation of the first shear crack in the NSM-4L90 beam, it was calculated the

24 $\Delta F / F^{NSM-4L90}$ ratio where ΔF is the increase of the load provided by SHCC plates and HCPs (

25 $\Delta F = F - F^{NSM-4L90}$), being $F^{NSM-4L90}$ the load capacity of the beam shear strengthened with CFRP laminates

26 applied according to the NSM technique, and F is the corresponding (for the same deflection) load capacity of the

1 other shear strengthened beams. $\Delta F / F^{NSM-4L90}$ (%) *vs.* corresponding deflection at loaded section relationship are

2 depicted in Figure 5(b), and its maximum value $(\Delta F / F^{NSM-4L90})_{max}$ is presented in Table 5.The values of the

3 F_{max} / F_{max}^{7S-R} ratio are also presented, where F_{max}^{7S-R} is the maximum load carrying capacity of the 7S-R beam.

4 The results show that the shear strengthening configuration formed by HCPs including CFRP laminates at 45° (SP-

5 3L45) was the most effective in terms of maximum load carrying capacity ($\Delta F_{max} / F_{max}^{0S-R}$), since an increase of

6 105% was obtained, while an increase of 87%, 77%, and 60% was determined for SP-4L90, NSM-4L90, and SP

7 beams, respectively.

8 The results in Figure 5(b) and Table 5 show that, for deflections higher than the one corresponding to the first shear

9 crack in the NSM-4L90 (2.7 mm) the adopted HCPs provided an increase in the beams load carrying capacity and

10 deflection performance. The decrease of the stiffness after the formation of the first shear crack in NSM-4L90 beam

11 was not so pronounced in the beams strengthened with HCPs.

12 By comparing the results of the SP-4L90 and SP-3L45 beams with those determined in the SP beam it is verified

13 that the CFRP laminates have contributed for the higher shear strengthening effectiveness of HCPs, since the

14 laminates have avoided the degeneration of the micro-cracks in the SHCC plates on macro-cracks, which had also a

15 positive effect in terms of the stiffness preservation of the beam and has also avoided the occurrence of premature

16 mixed shallow-semi-pyramid-plus-debonding failure modes registered currently when using the NSM-CFRP

17 technique. As reported in Bianco *et al.* (2011), the failure mode of a NSM CFRP laminate subjected to an imposed

18 end slip can be categorized into four groups: a) debonding, b) tensile rupture of laminate, c) concrete semi-pyramid

19 tensile fracture, and d) a mixed shallow semi-pyramid plus debonding failure mode (Figure 6). These modes of

20 failure are dependent on the relative mechanical and geometric properties of the materials involved.

21 The obtained experimental results show that SP-3L45 and SP-4L90 beams had a maximum load of 91% and 83% of

22 the maximum load of the 7S-R reference beam (F_{max}^{7S-R}), respectively, the one designed for flexural failure.

23

24

25

26

27

Detailed Analysis

0S-R beam

The 0S-R beam does not include any steel stirrups in the L_i span. During the loading of the beam, three cracks became visible at a load level of approximately 61kN. One of these cracks, of flexural-shear nature, initiated at 250mm from the support section, and the other two have formed at the center of the shear span. By increasing the load, the crack closer to the support section has converted in the shear failure crack, while the other cracks entered in a closing process. The crack pattern of the beam at a load of 61kN and at failure load (81kN) is represented in Figure 7(a) and 7(b), respectively. The maximum deflection at loaded section of the beam at failure load was 3.3mm.

NSM-4L90 beam

In the NSM-4L90 beam the first shear crack became visible at 260 mm from the support section, at the same load of the formation of the first shear crack in the reference beam (61kN). With the increase of load, more shear cracks were formed (Figure 7(c)) in the shear span. At a load of 126kN, cracks were formed along the longitudinal steel bars due to the dowel resistance offered by these bars to the propagation of the shear crack. Figure 7(d) shows that the laminate number 3 has crossed the shear failure crack. After the shear contribution of this laminate has been exhausted, a sudden failure has occurred with the widening of this crack. This was followed by the splitting of a bottom concrete cover region due to the shear deformation of the longitudinal bars that have offered dowel resistance to the propagation of the shear failure crack. An ultimate load of 143kN was achieved at a deflection of 8.2 mm. The maximum shear capacity of this beam was 77% greater than the one of the reference beam. The highest longitudinal strain reached in the CFRP laminates was recorded in the SG1 (Figure 3(b)) positioned at 81mm from the shear failure crack (marked with a circle in Figure 7(d)), and was approximately 0.66%, which corresponds to 40% of the ultimate strain of the CFRP. This strain value and all those herein reported are not necessarily the maximum values, since they are dependent of the relative position of the SGs with respect to the shear cracks. Figure 8 represents the curves of the load versus the strain in the SG where the maximum CFRP strain was registered in the strengthened beams. Up to the formation of the shear crack the maximum strain has increased almost linearly with the applied load, but did not exceed the strain value of 0.01% demonstrating that these CFRP laminates have marginal shear strengthening contribution during this stage, as expected. However, at the formation of the shear failure crack an abrupt increase of strain occurred.

SP beam

The SP beam was strengthened with two 720×300×20 mm SHCC plates (SP) with weight of around 7.7kg for each plate. During the loading process several micro-cracks have formed on the surface of the SHCC plates. Figure 7(e) and 6(f) shows the crack patterns a load level of about 124kN and at failure, respectively. At a load level of 124kN the cracks are visible by spraying oil (WD-40) on the surface of the SHCC plates. At a load of 130kN a shear failure crack became well visible and shear failure occurred. By applying the SHCC plates to the lateral faces of the beam, the weight and width of the SP beam's cross section became 5% and 27%, respectively, more than the one of the control beam. However, the shear resistance and the maximum deflection of the SP beam increased 60% and 92% compared to the control beam, respectively. In Figure 9 the crack patterns of 0S-R (gray color) and SP (black color-dash line) beams are compared at their corresponding maximum load. The shear failure crack in both beams has quite similar configuration, but SP beam presents much more flexural cracks, whose energy in its formation, as well as the resistance of the SHCC plate on the propagation of the shear failure crack have contributed for the significant increase in terms of load carrying capacity registered in this beam. Both beams presented a brittle behavior, with an abrupt load decay at peak load. As already mentioned, the SHCC was reinforced with 2% in volume of PVA fibers of 40μm diameter and 8mm length. The reinforcement mechanisms of these fibers were not able to absorb in a stable way the huge amount of energy released in the formation process of critical shear cracks.

SP-4L90 beam

The SP-4L90 beam had no steel stirrups in the L_i span, and was strengthened with HCPs applied on the beam's lateral faces in this span. The HCPs were formed by SHCC plates (SP) strengthened by four vertical ($\theta_f = 90°$) CFRP laminates (4L90) spaced at 180 mm (Figure 2(a)). Vertical lines in Figure 7(h) represent the position of the CFRP laminates. Like in SP beam, by increasing the load several micro-cracks have formed on the surface of the HCPs. This beam failed at a load level of 151kN with the formation of a shear failure crack between the two CFRP laminates closest to the point load (number 3 and 4), followed of the detachment of a part of the HCP that also included some concrete cover (Figure 7(g) and 7(h)). This alteration on the failure mode, assured by the HCP, has provided an increase of load carrying capacity (17%) and its corresponding deflection (33%) when compared to the SP beam, due to the contribution of the CFRP laminates. The highest longitudinal strain reached in the CFRP laminates was recorded by the SG6 (Figure 3(b)) at 15mm from a diagonal thin crack, and was approximately

1   0.21%, which corresponds to 12.7% of the ultimate strain of the CFRP laminate. The position of this strain gauge is

2   illustrated in Figure 7(h) by a circle. The premature detachment of the HCPs justifies the relatively low collaboration

3   of the CFRP laminates for the shear strengthening, demonstrated by the too low maximum strain registered (Figure

4   8). This indicates that for a higher mobilization of the strengthening potentialities of the CFRP laminates, the HCPs

5   should be not only bonded to the substrate with an adhesive but also fixed with chemical anchors (Esmaeeli *et al.*

6   2014).

7

8   *SP-3L45 beam*

9   Although the shear CFRP strengthening ratio has been the same in the SP-3L45 and SP-4L90 beams (

10    $\rho_{fw}^{SP-4L90} = \rho_{fw}^{SP-3L45} = 0.10\%$), the inclination of the CFRP laminates was different, leading to differences on the

11   contribution of these laminates for the shear strengthening of this type of beams. The HCPs of the SP-3L45 beam

12   were formed by SHCC plates (SP) strengthened with three $\theta_f = 45°$ CFRP laminates (3L45) spaced at 250mm

13   (Figure 2(b)). The lines in Figure 7(i) represent the position of the CFRP laminates. The first shear crack was

14   detected at a load level of 76kN. Figure 7(i) shows the crack pattern of this beam at a load level of 123 kN, where it

15   is visible the formation of flexural and flexural-shear cracks. The failure of the beam is governed by the detachment

16   of the HCPs (Figure 7(j)), each one bringing together part of the concrete cover of the lateral surface of the beam,

17   which is a failure mode already reported in Dias and Barros (2013) when high percentage of CFRP laminates are

18   used on the shear strengthening of RC beams. Like in the SP-4L90 beam, the load carrying capacity of the SP-3L45

19   beam was limited by this typical failure mode. However, the better orientation of the CFRP laminates in relation to

20   the shear cracks formed in the concrete core of the SP-3L45 beam has assured a larger area of concrete fracture

21   during the detachment process of the HCPs (as is clearly visible when Figure 7(g) and 7(j) are compared), which

22   caused a higher load carrying capacity and its corresponding deflection in this beam, when compared to the SP-4L90

23   beam. In fact failure occurred at a load level of 166kN, indicating an increase of 105%, 16%, 28%, and 10%

24   compared with 0S-R, NSM-4L90, SP, and SP-4L90, respectively. The maximum longitudinal strain reached in the

25   CFRP laminates (SG3, Figure 3(b)) was approximately 0.35%, which corresponds to 21% of the ultimate strain of

26   the CFRP. Like already pointed out for the SP-4L90 beam, the detachment of the HCPs also occurred in the SP-

27   3L45 beam has avoided the mobilization of the shear strengthening potentialities of the CFRP laminates.

28

7S-R beam

2   As expected, the beam shear reinforced in the shear span with steel stirrups of $\phi8@100$ (7S-R) has failed in bending

3   with the yielding of the flexural reinforcement (at 182kN), followed by the concrete crushing (at about 170kN and a

4   deflection of 20 mm) in the loaded zone (Figure 7(k)).

5

6   **Numerical Simulations and Parametric Study**

7   *Constitutive model and its predictive performance*

8   The three dimensional multi-fixed smeared crack model described in Ventura-Gouveia (2011), implemented in the

9   FEM-based computer program FEMIX (Sena-Cruz *et al.* 2007), was used in the numerical simulations carried out in

10   this work. To simulate the crack initiation and the fracture mode I propagation of plain concrete and SHCC, the tri-

11   linear tension-softening diagram represented in Figure 10 was adopted (Sena-Cruz 2004), which is defined by the

12   parameters α_i and ξ_i, relating stress with strain at the transitions between the linear segments that compose this

13   diagram. The ultimate crack strain, $\varepsilon_{n,u}^{cr}$, is defined as a function of the parameters α_i and ξ_i, the fracture energy,

14   G_f^I, the tensile strength, $\sigma_{n,1}^{cr} = f_{ct}$, and the crack bandwidth, l_b (Sena Cruz 2004). The values of this diagram

15   are indicated in Table 6 and 7 for plain concrete and SHCC, respectively. These tables also include the data

16   necessary to define the shear-softening diagram that simulates the degradation of crack shear stress transfer after

17   crack initiation (Ventura-Gouveia *et al.* 2008; Ventura-Gouveia 2011; Barros *et al.* 2013) represented in Figure 11,

18   which is defined by the initial shear fracture modulus, $D_{t,1}^{cr}$, and the peak crack shear strain, $\gamma_{t,p}^{cr}$, obtained using

19   the crack shear strength (from the input data), $\tau_{t,p}^{cr}$, and the initial shear fracture modulus, $D_{t,1}^{cr}$. The ultimate crack

20   shear strain, $\gamma_{t,u}^{cr}$, depends on the crack shear strength, $\tau_{t,p}^{cr}$, on the shear fracture energy, $G_{f,s}$, and on the crack

21   bandwidth, l_b (Ventura-Gouveia 2011). More details of the remaining variables of this constitutive model can be

22   found in Ventura-Gouveia (2011) and Barros *et al.* (2013). The data for the shear softening diagram of plain

23   concrete was determined by fitting as best as possible the force-deflection relationship registered in the control beam

24   tested experimentally (0S-R), while for the SHCC this data was obtained by simulating the SP beam. For the

25   analysis of the remaining beams of the experimental program the values of the constitutive model applied to each

26   intervening material were preserved constant.

Figure 12 represents the finite element mesh adopted for the RC beam. The mesh was adopted after some preliminary simulations in terms of assuring mesh objectivity of the results. In the simulations this finite element mesh was only altered in order to take into account the strengthening provided by NSM laminates (NSM-4L90 beam), the SHCC panel (SP beam), HCPs (SP-4L90 and SP-3L45 beans), and the use of more steel stirrups (7S-R beam).

Only half of the full size beam was modeled, taking advantage of the symmetry of the beams in order to reduce the computational time of the numerical simulations. Serendipity 8 nodes solid elements with 2×2×2 Gauss-Legendre integration scheme were used for both the concrete and SHCC (three degrees-of-freedom per node). The steel stirrups, longitudinal steel bars and CFRP laminates were modeled with 2-node 3D embedded cables elements (one degree-of-freedom per node) with two Gauss-Legendre integration points. Perfect bond to the surrounding medium was assumed. The tested beams showed that no slip occurred between concrete substrate and SHCC plates, thus the assumption of perfect bond between substrate and SHCC plates was assumed.

To model the behavior of the longitudinal and transversal steel bars, the stress-strain relationship represented in Figure 13 was adopted (Sena-Cruz 2004). The curve (under compressive or tensile loading) is defined by the points PT1=$(\varepsilon_{sy}, \sigma_{sy})$, PT2=$(\varepsilon_{sh}, \sigma_{sh})$, and PT3=$(\varepsilon_{su}, \sigma_{su})$, and a parameter P that defines the shape of the last branch of the curve. Unloading and reloading linear branches with slope $E_s = (\sigma_{sy} / \varepsilon_{sy})$ are assumed in the present approach. The values of the parameters of the constitutive model for the steel bars are indicated in Table 8. For modeling the NSM CFRP laminates, a linear elastic stress-strain relationship was adopted.

The experimental and the numerical relationships between the applied load and the deflection at the loaded section for the tested beams are compared in Figure 14. The crack pattern of these beams at the end of the analysis is represented in Figure 15. These two figures show that the numerical model is able of capturing with enough accuracy the deformational response of the beams, as well as the localization and profile of the failure cracks. For the beams strengthened with SHCC/HCP, the crack pattern is represented for the concrete substrate of the lateral surface, as well as for the SHCC/HCP. In Figure 15 a section view of the crack pattern of the SP-3L45 beam is also represented in order to demonstrate the capability of the model to reproduce the localization of failure cracks at the concrete region close to the HCP/beam interface, as already reported.

Parametric Study for Assessing the Potentialities of the Developed Strengthening Technique

The computer program, whose good predictive performance for the simulation of the behavior of the structures under consideration was confirmed in the previous section, was adopted to execute a parametric study for the evaluation of the influence on the load carrying capacity and failure mode of the following parameters: arrangement of CFRP laminates and its shear strengthening ratio; the use of mechanical anchors for fixing the HCP to the RC beam.

The arrangement of the steel reinforcement, the material properties of concrete, SHCC and CFRP laminates, the support and load conditions, and the finite element mesh were the same of the ones adopted in the numerical simulations of the previous section. The beams simulated in the parametric study are shown in Figure 16. It should be noted that at the right of the loaded section all the beams have the same shear reinforcement configuration. Two shear strengthening ratios ($\rho_{fw} = 0.10\%$ and $\rho_{fw} = 0.20\%$) and four arrangements of CFRP laminates (30°, 45°, 60°, 90°) were studied. To prevent premature debonding of the HCPs and also to provide some confinement of the concrete core, the efficiency of using mechanical anchors for fixing HCP to the beam was also evaluated. A hybrid strengthening configuration composed of HCP for the shear reinforcement and longitudinal NSM CFRP laminates for the flexural reinforcement was also investigated for assuring a relatively high increase of load carrying capacity of RC beams. It was assumed that the longitudinal CFRP laminates had the same material properties of CFRP laminates for the shear strengthening. The designation of the beams composing this parametric study is indicated in Figure 16.

Influence of Strengthening Configuration and Percentage of CFRP Laminates:

Figure 17 compares the relationship between load and deflection curves at loaded section obtained for two different values of the shear strengthening ratio ($\rho_{fw} = 0.10\%$ and $\rho_{fw} = 0.20\%$) and four types of shear strengthening arrangements of the CFRP laminates (30°, 45°, 60°, 90°). The HCPs of SP-3L30, SP-3L45, SP-4L60, and SP-4L90 beams were strengthened with $\rho_{fw} = 0.10\%$, while the HCPs of SP-5L30, SP-5L45, SP-7L60, and SP-7L90 beams were strengthened with $\rho_{fw} = 0.20\%$. Figure 18 also compares the crack patterns of these beams (at the end of the last converged load increment). The crack patterns revealed that by increasing the CFRP percentage the failure mode shifted to detachment of the HCPs, that it can be avoided by using mechanical anchors.

1

2

3 *Influence of Mechanical Anchors:*

4 Figure 19 compares the load-deflection curves obtained for two different ways to apply the HCPs to the concrete

5 substrate of the lateral faces of the beam. In the first case, it is assumed the HCPs have been attached using an

6 adhesive epoxy (full bond), while in the second case the HCPs are bonded using epoxy adhesive and fixed with 12

7 mechanical anchors. Figure 16 shows the position of the bolts. The diameter of the bolts is assumed 12 mm and a

8 torque of 30N.m is applied to tighten the bolts on both sides of the beam. The mechanical anchors can prevent

9 premature detachment of the HCPs, and provide confinement to the concrete core whose level depends on the torque

10 and arrangement of the bolts. The bolts are modeled with 3D two-node truss elements, and torque was simulated by

11 applying a temperature decrease of -23°C in these elements, evaluated according to the following equations:

$$F = \frac{\tau}{r} \qquad\qquad F = \frac{30}{0.006} = 5000 \ N \qquad\qquad (2)$$

$$\sigma = \frac{F}{A} \qquad\qquad \sigma = \frac{5000}{113} = 44.2 MPa$$

$$\varepsilon = \frac{\sigma}{E} = T.\alpha \qquad\qquad \varepsilon = \frac{44.2}{200000} = T \times 10^{-5}$$

12 where τ is torque (N.m), and r, A, and E are the radius, cross sectional area, and elasticity modulus of the bolt (6

13 mm, 113 mm^2, 200GPa), respectively. In this equations T and α are temperature and temperature coefficient,

14 respectively.

15 By applying the mechanical anchors, the load carrying capacity of the beams increased and the failure mode was

16 changed from premature detachment of the HCPs to flexural failure (Figure 20).

17

18 *Flexural Strengthening of the Beams:*

19 Based on the results in the previous section, by fixing with bolts the HCPs reinforced with the higher percentage of

20 CFRP laminates, the beams have failed in bending, which avoided accessing the full strengthening potential of these

21 HCPs. Thus, to access the shear strengthening effectiveness of these HCPs, it is essential to increase the flexural

22 capacity of the beams. For this purpose, the beams were also strengthened in bending by using two longitudinal

23 CFRP laminates (Figure 16) of 20×1.4 mm^2 cross sectional area and material properties equal to those used in the

HCPs. Figure 21 and 22 compare the relationship between load and deflection at the loaded section, as well as the crack patterns of the simulated beams. As the results show, this hybrid strengthening arrangement has provided a significant increase of the beam's load carrying capacity, with the highest increase registered in the beam shear strengthened with HCPs reinforced with laminates at 45°. The laminates at 60° are more effective than laminates at 90°.

Conclusions

The effectiveness of Hybrid Composite Plates (HCPs) for the shear strengthening of RC beams was evaluated by carrying out an experimental program formed by a control beam (0S-R), a beam reinforced with strain hardening cement composite (SHCC) plates (SP), a beam shear strengthened according to the NSM technique (NSM-4L90), and two beams shear strengthened with HCPs (SP-4L90 with vertical CFRP laminates, and SP-3L45 with 45° laminates). From the obtained results it was verified that, in the absence of steel stirrups, the HCPs have provided a maximum increase of 105% of shear capacity, when the control beam is considered for comparison purposes. The 0S-R, SP, and NSM-4L90 beams failed in shear, while the failure mode of SP-4L90 and SP-3L45 beams was a combination of shear failure and detachment of the HCPs. The effectiveness level of the HCP technique was limited by the tensile strength of the concrete substrate of the RC beams, since at failure, a concrete cover layer of an average thickness that varied between 5 and 10 mm was attached to the HCPs. The detachment of HCPs has avoided the mobilization of the shear strengthening potentialities of the CFRP laminates. However, the results have shown that for deflections higher than the one corresponding to the formation of the first shear crack in the beam strengthened with NSM technique (NSM-4L90), the adopted HCPs have increased the beam's load carrying capacity and deflection performance. The SHCC surrounding the CFRP laminates in the HCP has offered effective resistance to the degeneration of micro-cracks on macro-cracks., which has avoided the occurrence of premature mixed shallow-semi-pyramid-plus-debonding failure modes registered currently when using the NSM-CFRP technique.

This technique can be used for the shear strengthening of deep RC beams and walls, mainly for those walls pertaining to buildings that need to be strengthened against to lateral loads like those typical of seismic events and also for repairing of RC beams that have previously failed in shear.

The capability of a FEM-based computer program to predict with high accuracy the behavior of this type of structures up to its collapse was studied. The shear crack softening diagram available in the multi-directional fixed smeared crack model implemented in the FEMIX computer program, allowed to predict the load carrying capacity, crack patterns and failure modes of the tested beams.

To evaluate the influence on the beam's load carrying capacity of the shear strengthening arrangement and ratio of CFRP laminates that reinforce the HCPs, as well as the effectiveness of mechanical anchors in terms of avoiding the premature detachment of the HCPs, a parametric study was carried out by FEMIX computer program. By increasing the shear strengthening ratio of CFRP laminates, and fixing the HCPs to the beam's concrete substrate by mechanical anchors, failure mode can be shifted from shear failure and detachment of the HCPs to flexural failure. It was also verified that HCP's with laminates at 45° was the most effective arrangement in terms of shear strengthening with the proposed technique. The hybrid technique composed of HCPs for the shear strengthening and NSM CFRP laminates for the flexural strengthening was capable of increasing significantly the load carrying capacity of RC beams by highly mobilizing the potentialities of these reinforcement systems.

References:

Abdel-Jaber, M. S., Walker, P.R. and Hutchinson, A.R. (2003). "Shear strengthening of reinforced concrete beams using different configurations of externally bonded carbon fiber reinforced plates", *Materials and Structures*, Vol. 36, No. 5, pp. 291-301.

Barros, J. A. O., Baghi, H., Dias, S.J.E. and Ventura-Gouveia. A. (2013). "A FEM-based model to predict the behaviour of RC beams shear strengthened according to the NSM technique", *Engineering Structures*, Vol. 56, pp. 1192-1206.

Bianco, V., Monti, G. and Barros, J.A.O. (2011). "Theoretical model and computational procedure to evaluate the NSM FRP strips shear strength contribution to a RC beam", *Structural Engineering*, Vol. 137, No. 11, pp. 1359-1372.

Chaallal, O., Mofidi, A., Benmokrane, B. and Neale, K. (2011). "Embedded Through-Section FRP Rod Method for Shear Strengthening of RC Beams: Performance and Comparison with Existing Techniques", *Composites for Construction*, Vol. 15, No. 3, pp. 374-383.

Costa, I. G. and Barros, J.A.O. (2010). "Flexural and shear strengthening of RC beams with composite materials – The influence of cutting steel stirrups to install CFRP strips", *Cement and Concrete Composites* , Vol. 32, No. 7, pp. 544-553.

Dias, S. J. E. and Barros, J.A.O. (2010). "Performance of reinforced concrete T beams strengthened in shear with NSM CFRP laminates", *Engineering Structures*, Vol. 32, pp. 373-384.

Dias, S. J. E. and Barros, J.A.O. (2013). "Shear strengthening of RC beams with NSM CFRP laminates: Experimental research and analytical formulation", *Composite Structures*, Vol. 99, pp. 477-490.

Esmaeeli, E., Barros, J. and Mastali, M. (2012). Effects of curing conditions on crack bridging response of PVA reinforced cementitious matrix, *8th RILEM international symposium on fibre reinforced concrete: challenges and opportunities (BEFIB2012)*. Guimaraes, Portugal.

Esmaeeli, E., Barros, J.A.O. and Baghi, H. (2013a). Hybrid Composite Plates (HCP) for Shear Strengthening of RC Beams, *11th International symposium on fiber reinforced polymers for reinforced concrete structures (FRPRCS11).* Guimaraes, Portugal.

Esmaeeli, E., Barros, J.A.O., Baghi, H. and Sena-Cruz, J. (2014). Development of Hybrid Composite Plate (HCP) for the Repair and Strengthening of RC Elements, *3rd International RILEM Conference on Strain Hardening Cementitious Composites (SHCC3*-Delft), Delft University, Netherland.

Esmaeeli, E., Barros, J.A.O., Sena-Cruz, J., Varum, H. and Melo, J. (2015). "Assessment of the efficiency of prefabricated hybrid composite plates (HCPs) for retrofitting of damaged interior RC beam–column joints", *Composite Structures*, Vol. 119, pp. 24-37.

Esmaeeli, E., Manning, E. and Barros, J.A.O. (2013b). "Strain hardening fibre reinforced cement composites for the flexural strengthening of masonry elements of ancient structures", *Construction and Building Materials*, Vol. 38, pp. 1010-1021.

European Standard (1990). Metallic materials Tensile testing. Part 1: Method of test (at ambient temperature), *EN 10002-1*, Brussels, Belgium: European Committee for Standardization.

European Standard (1996). Plastics - Determination of tensile properties - Part 2: Test conditions for moulding and extrusion plastics, *ISO 527-2*, London South Bank University, International Organization for Standardization (ISO).

European Standard (1997). Plastics - Determination of tensile properties Part 5: Test conditions for unidirectional fibre-reinforced plastic composites, *ISO 527-5*, Geneva (Switzerland), International Organization for Standardization (ISO).

European standard (2000). Concrete - Part 1: Specification, performance, production and conformity, *EN206-1*, CEN: European Committee for Standardization.

Khalifa, A., Gold, W.J., Nanni, A. and Aziz, A. (1998). "Contribution of externally bonded FRP to shear capacity of RC flexural members", *Composites for Construction*, Vol. 2, No. 4, pp. 195-203.

Li, V. C. (1998). "Engineered Cementitious Composites for Structural Applications", *Materials in Civil Engineering*, Vol. 10, pp. 66-69.

Lorenzis, L. and Nanni, A. (2001). "Shear Strengthening of Reinforced Concrete Beams with Near-Surface Mounted Fiber-Reinforced Polymer Rods", *ACI Structural Journal*, Vol. 98, pp. 60-68.

Orosz, K., Blanksvärd, T., Täljsten, B. and Fischer, G. (2013). "Crack development and deformation behaviour of CFRP-reinforced mortars", *Nordic Concrete Research*, Vol. 48, pp. 49-69.

Parra-Montesinos, G. and Wight, J.K. (2000). "Seismic response of exterior RC column-to steel beam connections", *Structural Engineering*, Vol. 126, pp. 1113-1121.

Rezazadeh, M., Costa, I. and Barros, J. (2014). "Influence of prestress level on NSM CFRP laminates for the flexural strengthening of RC beams", *Composite Structures*, Vol. 116, pp. 489-500.

Saafan, M. A. A. (2006). "Shear Strengthening of Reinforced Concrete Beams Using GFRP Wraps", *Acta Polytechnica*, Vol. 46, pp. 24-32.

Sena-Cruz, J. M. (2004). *Strengthening of concrete structures with near-surface mounted CFRP laminate strips*, PhD Thesis, University of Minho, Guimaraes, Portugal.

Sena-Cruz, J.M., Barros, J.A.O., Azevedo, A.F.M. and Ventura-Gouveia, A. (2007). Numerical simulation of the nonlinear behavior of RC beams strengthened with NSM CFRP strips, Proceedings of CMNE/CILAMCE Congress, FEUP, Porto, Portugal.

Shang, Q. and Zijl, G.V. (2007). "Characterising the shear behaviour of strain-hardening fibre-reinforced cement-based composites", *South African Institution of Civil Engineering*, Vol. 35, pp. 16-23.

Su, R. K. L., Siu, W.H. and Smith, S.T. (2010). "Effects of bolt-plate arrangements on steel plate strengthened reinforced concrete beams", *Engineering Structures*, Vol. 32, pp. 1769-1778.

Ventura-Gouveia, A. (2011). *Constitutive models for the material nonlinear analysis of concrete structures including time-dependent effects*, PhD Thesis, University of Minho, Guimaraes, Portugal.

Ventura-Gouveia, A., Barros, J., Azevedo, A. and Sena-Cruz, J. (2008). Multi-fixed smeared 3d crack model to simulate the behavior of fiber reinforced concrete structures, *CCC 2008 - Challenges for Civil Construction*, Porto, Portugal.

1 **LIST OF FIGURE CAPTIONS**

2

3 **Figure 1.** Geometry and reinforcement arrangement of the concrete beams (dimensions in mm)

4 **Figure 2.** Configurations of the HCPs (dimensions in mm)

5 **Figure 3.** Monitoring system- position of the: a) LVDTs; and b) strain gauges in CFRP laminates (dimensions in

6 mm)

7 **Figure 4.** The envelope and the average tensile stress versus crack opening displacement (COD) obtained in notched

8 specimens (Esmaeeli *et al.* 2013b)

9 **Figure 5.** a) Force vs. deflection at the loaded-section, and b) $\Delta F / F^{NSM-4L90}$ vs. deflection at the loaded-section for

10 the beams strengthened with SHCC plates and HCPs

11 **Figure 6.** The mode of failure of an NSM CFRP laminate subjected to an imposed end slip (Bianco *et al.* 2011)

12 **Figure 7.** Crack patterns and failure modes of the tested beams

13 **Figure 8.** Force vs. strain in monitored laminates in SGs where the maximum strains were registered

14 **Figure 9.** Crack patterns of the 0S-R (gray color) and SP (black color-dash line) at failure load

15 **Figure 10.** Tri-linear stress-strain diagram to simulate the fracture mode I crack propagation ($\sigma_{n,2}^{cr} = \alpha_1 \sigma_{n,1}^{cr}$,

16 $\sigma_{n,3}^{cr} = \alpha_2 \sigma_{n,1}^{cr}$, $\varepsilon_{n,2}^{cr} = \xi_1 \varepsilon_{n,u}^{cr}$, $\varepsilon_{n,3}^{cr} = \xi_2 \varepsilon_{n,u}^{cr}$) (Sena-Cruz 2004)

17 **Figure 11.** Diagrams to simulate the relationship between the crack shear stress and crack shear strain component,

18 and possible shear crack statuses (Barros *et al.* 2013)

19 **Figure 12.** Geometry, mesh and support condition (dimensions in mm)

20 **Figure 13.** Uniaxial constitutive model for the steel bars (Sena-Cruz 2004)

21 **Figure 14.** Comparison between experimental and numerical relationships of force vs. deflection at the loaded
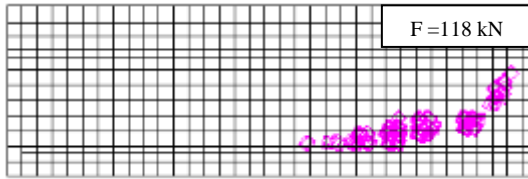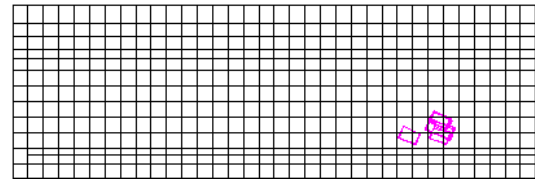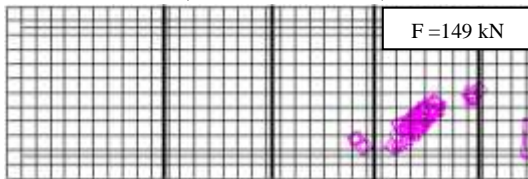
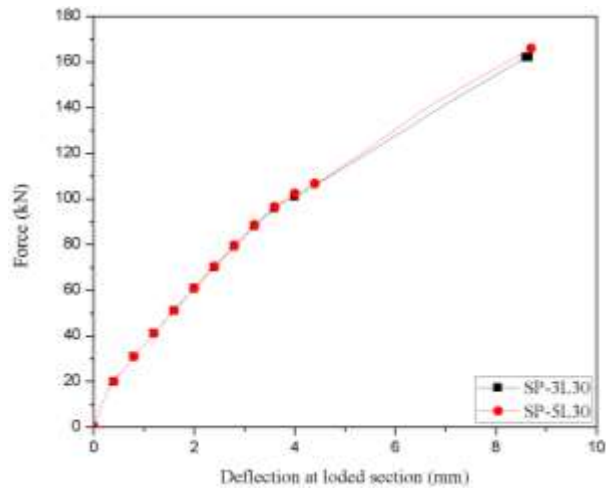22 section

23 **Figure 15.** Crack patterns of the beams (pink color: crack completely open; red color: crack in the opening process;

24 cyan color: crack in the reopening process; green color: crack in the closing process; blue color: closed crack)
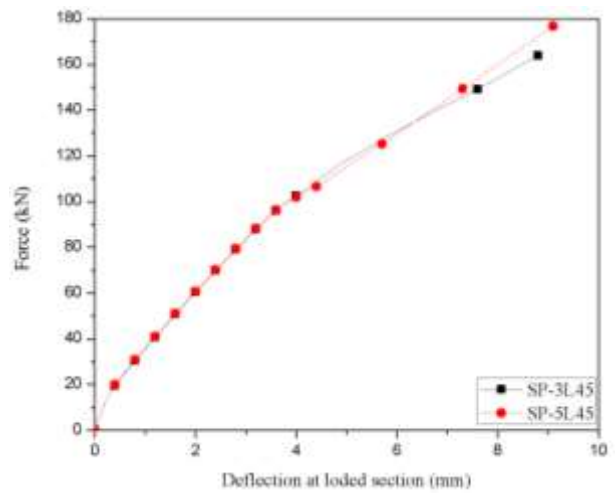
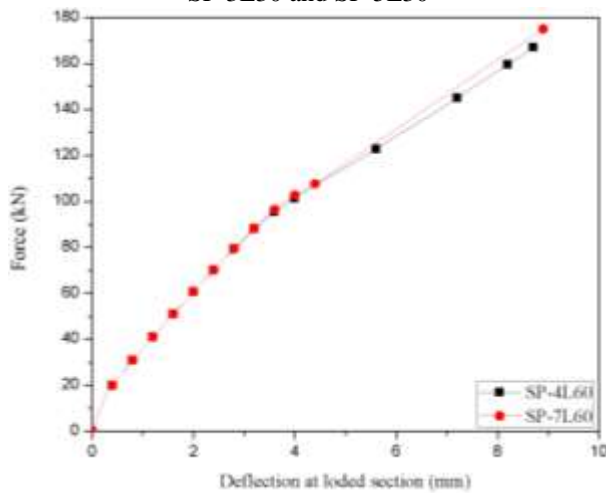25 **Figure 16.** Strengthening scheme of the specimens (dimensions in mm)

26 **Figure 17.** Influence of inclination and percentage of the CFRP laminates on the relationship between the force and

27 the deflection at loaded section

Force

A

ø8@100

Ø10

Ø20

300

20

150

Sec. A-A

L_i =800

L_r=1400

A

Type A

Force

B

A

300

150

Sec. B-B

L_i =800

L_r=1400

B

A

Type B

1   **Figure 1.** Geometry and reinforcement arrangement of the concrete beams (dimensions in mm)

a) SHCC plate with vertical CFRP laminates (θ_f =90°)

b) SHCC plate with inclined CFRP laminates (θ_f =45°)

9 11

CFRP Laminates

Epoxy adhesive

HCP RC beam

Sec. A-A

CFRP
laminate
10x1.4mm² 4mm

Epoxy adhesive
for bonding the
CFRP laminates to
the SHCC plate

9
11

Epoxy adhesive

HCP

RC beam

Sec. B-B
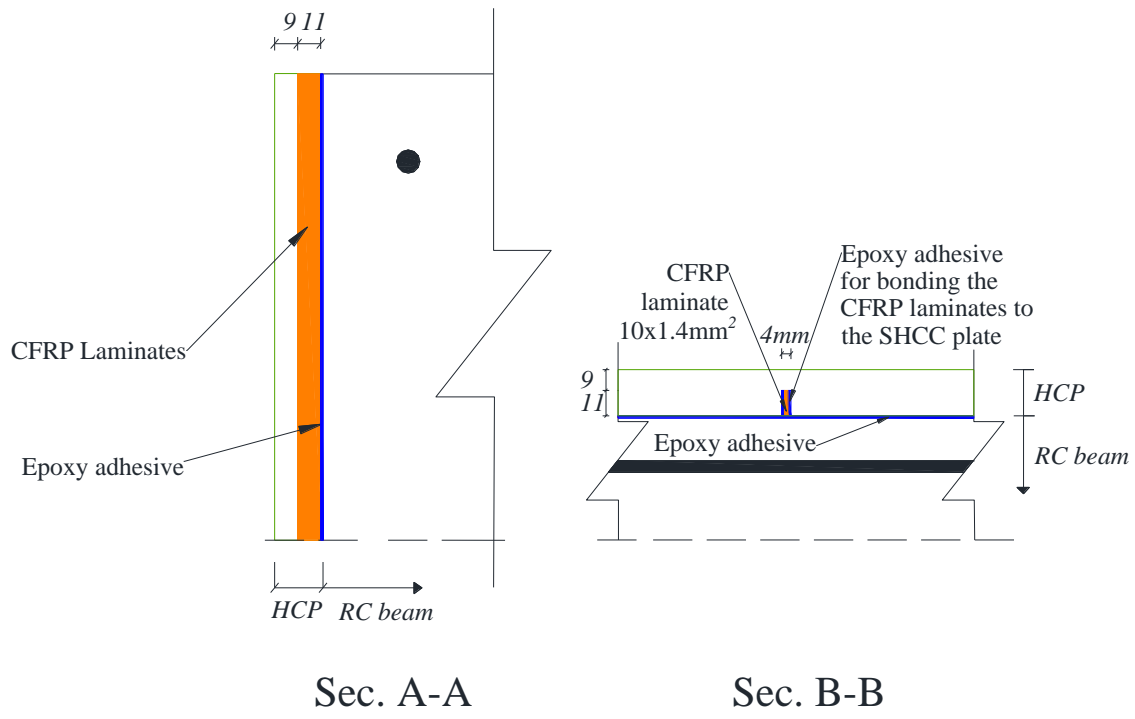
c) Position of the laminates inside the SHCC plate

1 **Figure 2.** Configurations of the HCPs (dimensions in mm)
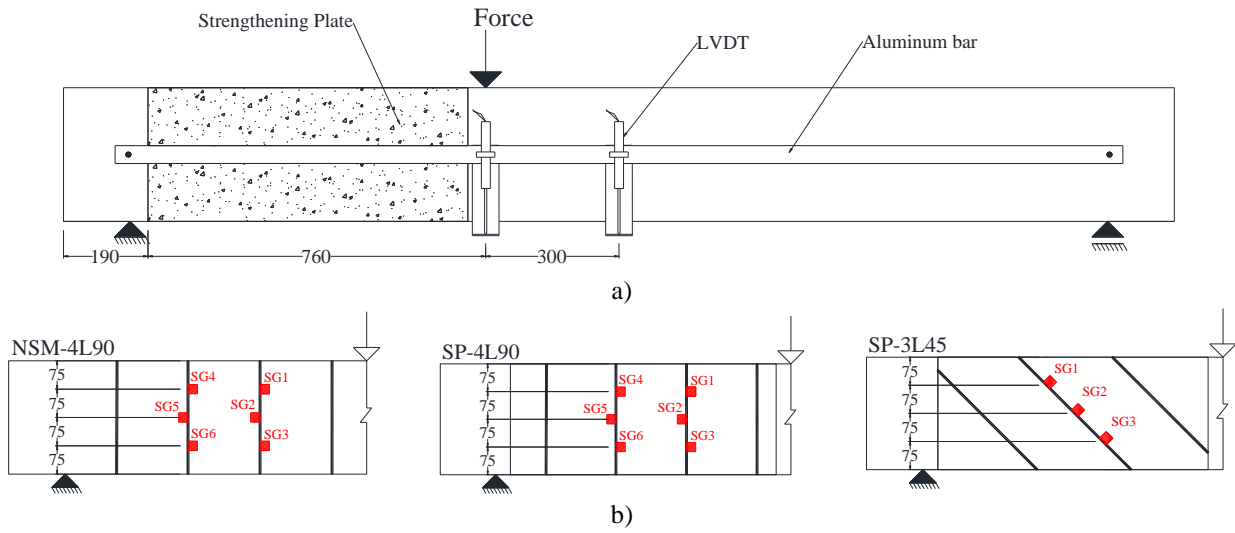
Figure 3. Monitoring system- position of the: a) LVDTs; and b) strain gauges in CFRP laminates (dimensions in mm)

Figure 4. The envelope and the average tensile stress versus crack opening displacement (COD) obtained in notched specimens (Esmaeeli *et al.* 2013b)

a)

b)

Figure 5. a) Force vs. deflection at the loaded-section, and b) $\Delta F / F^{NSM-4L90}$ vs. deflection at the loaded-section for the beams strengthened with SHCC plates and HCPs

a) Debonding   b) Strip tensile rupture   c) Concrete semi-pyramidal fracture   d) Mixed shallow-semi-pyramid plus debonding
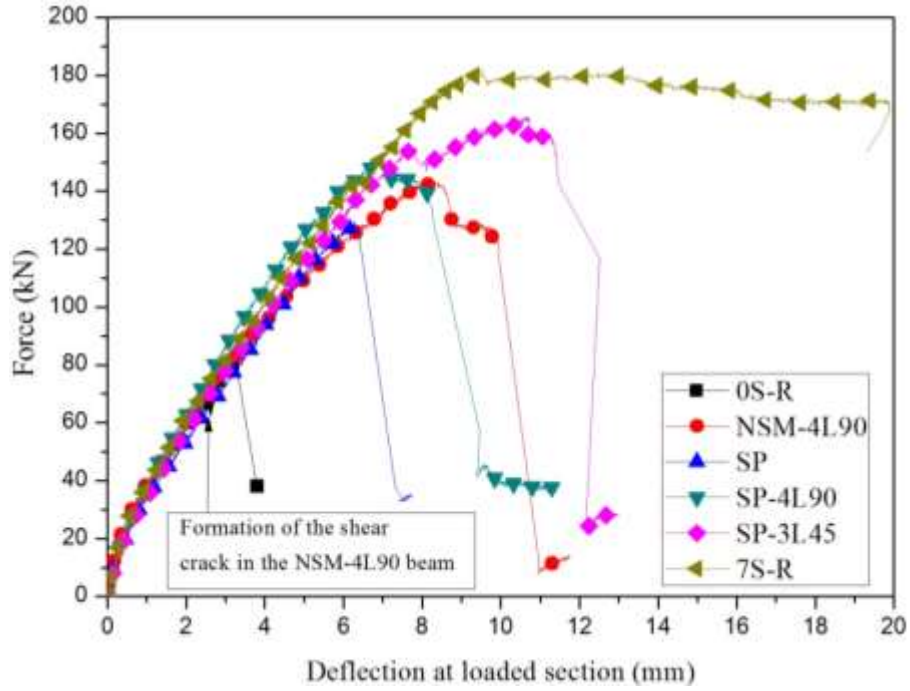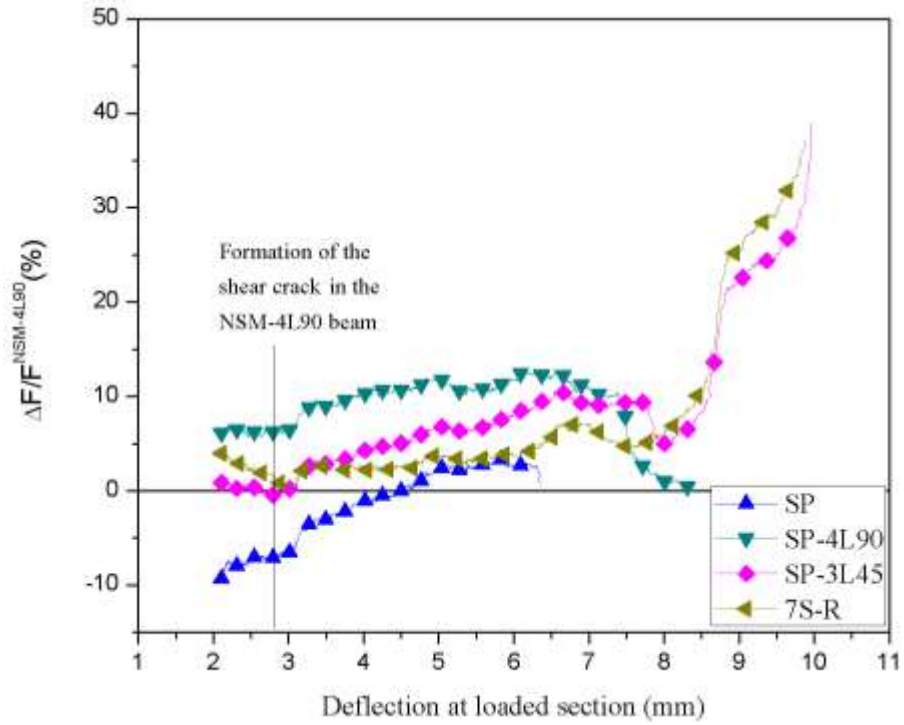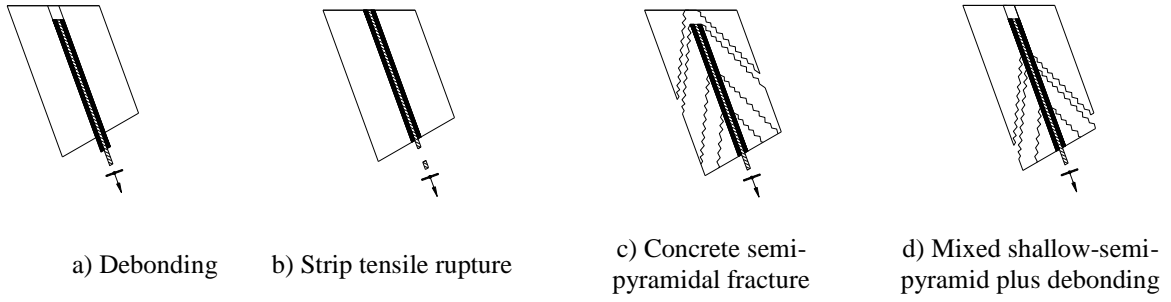
1   **Figure 6.** The mode of failure of an NSM CFRP laminate subjected to an imposed end slip (Bianco *et al.* 2011)
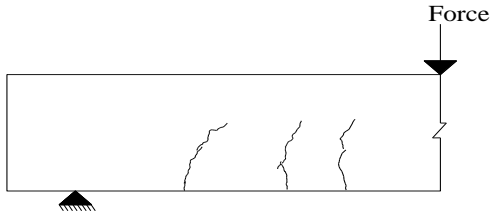
a) Crack pattern at the load level of 61 kN of the 0S-R beam

b) Crack pattern at failure load of the 0S-R beam
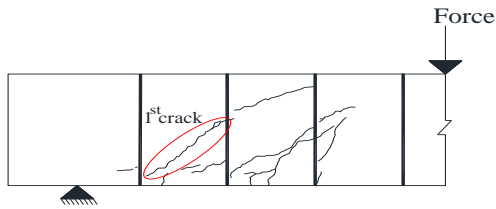
c) Crack pattern at the load level of 126kN of the NSM-4L90 beam
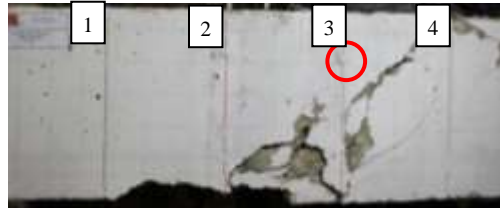
d) Crack pattern at failure load of the NSM-4L90 beam

e) After spraying the oil on the surface of the SHCC plates of SP beam

f) Crack pattern at failure load of the SP beam

g) Detachment of the HCPs in SP-4L90 beam
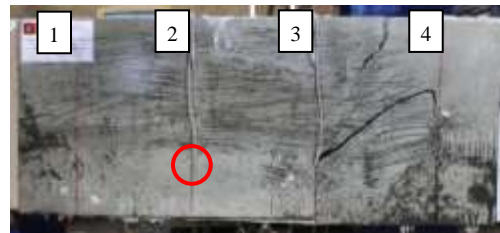
h) Failure mode of the SP-4L90 beam

i) Crack pattern in the lateral surface of SP-3L45 beam at the load level of 123 kN

j) Crack pattern in the bottom surface at failure load of SP-3L45 beam

k) 7S-R beam
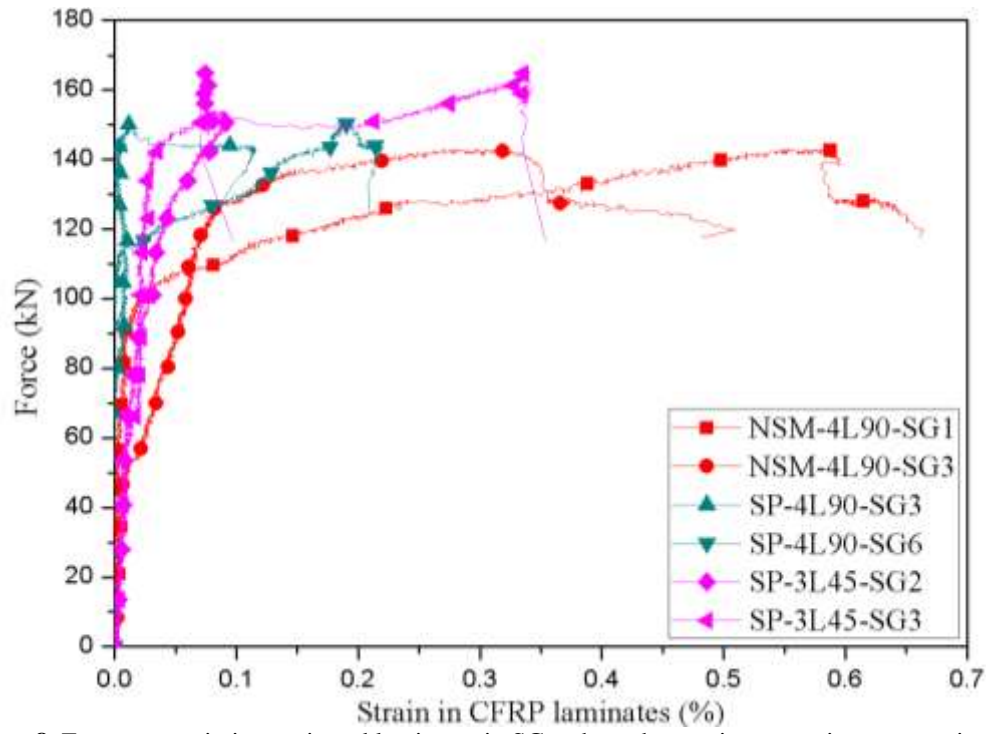
Figure 7. Crack patterns and failure modes of the tested beams

1

1
2   **Figure 8.** Force vs. strain in monitored laminates in SGs where the maximum strains were registered
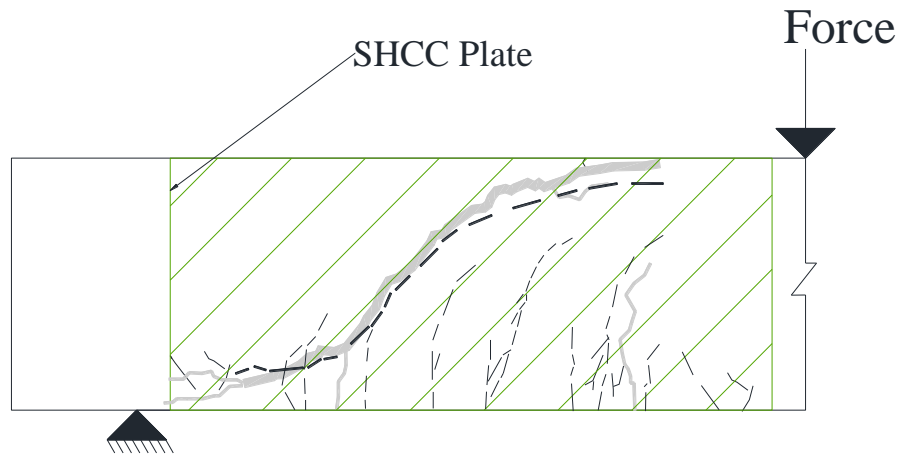
Figure 9. Crack patterns of the 0S-R (gray color) and SP (black color-dash line) at failure load
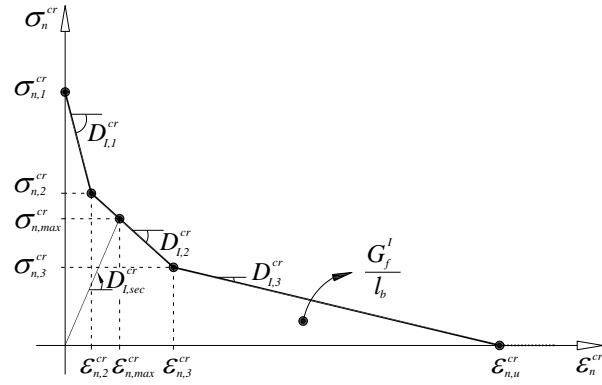
Figure 10. Tri-linear stress-strain diagram to simulate the fracture mode I crack propagation ($\sigma_{n,2}^{cr} = \alpha_1 \, \sigma_{n,1}^{cr}$, $\sigma_{n,3}^{cr} = \alpha_2 \, \sigma_{n,1}^{cr}$, $\varepsilon_{n,2}^{cr} = \xi_1 \, \varepsilon_{n,u}^{cr}$, $\varepsilon_{n,3}^{cr} = \xi_2 \, \varepsilon_{n,u}^{cr}$) (Sena-Cruz 2004)
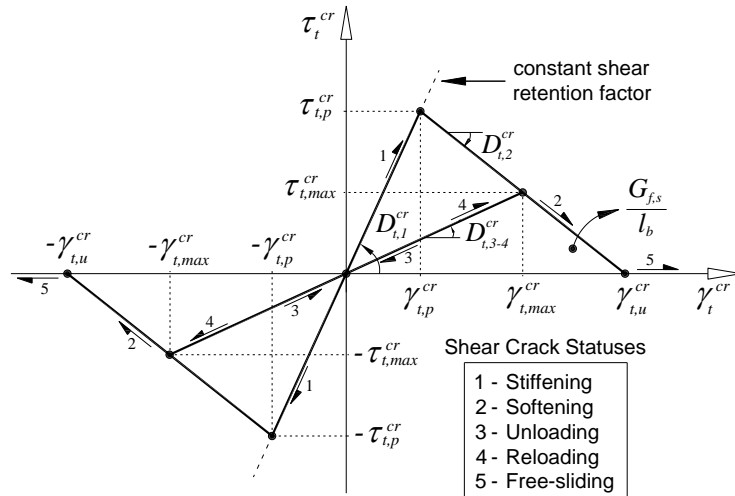
Figure 11. Diagrams to simulate the relationship between the crack shear stress and crack shear strain component, and possible shear crack statuses (Barros *et al.* 2013)
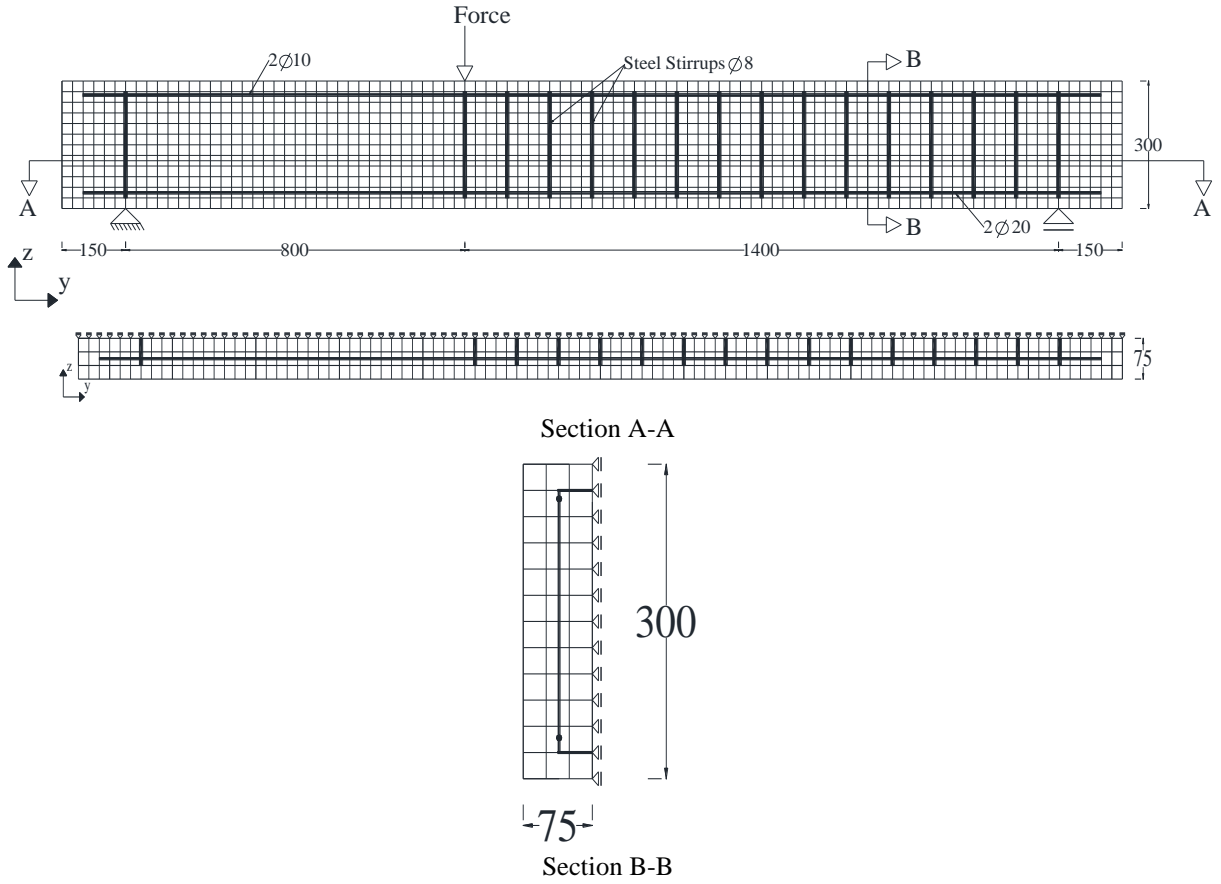
Figure 12. Geometry, mesh and support condition (dimensions in mm)
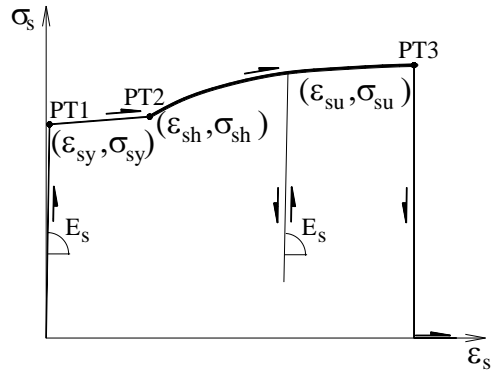
Figure 13. Uniaxial constitutive model for the steel bars (Sena-Cruz 2004)
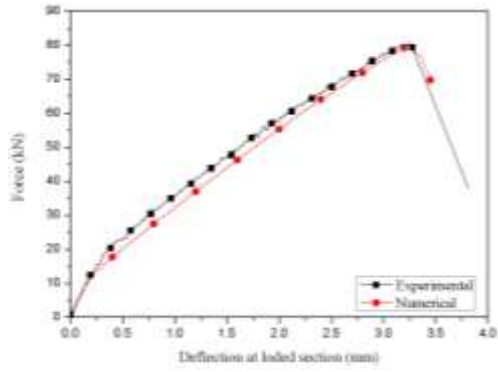
(a) 0S-R
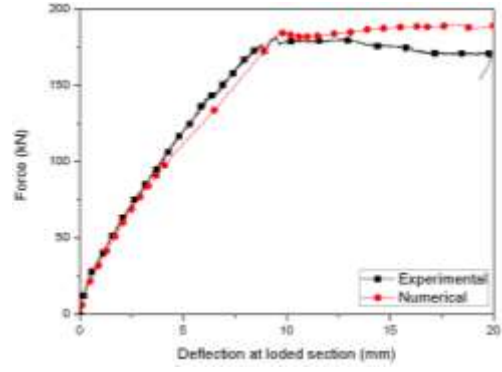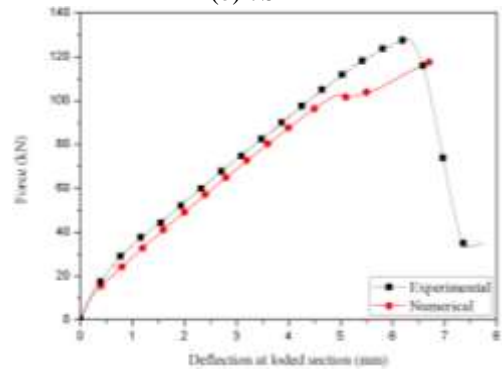
(b) 7S-R

(c) NSM-4L90

(d) SP
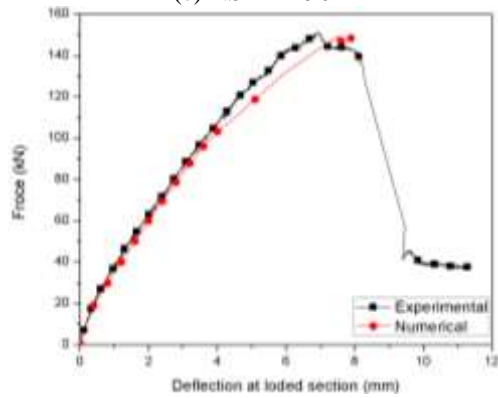
(e) SP-4L90
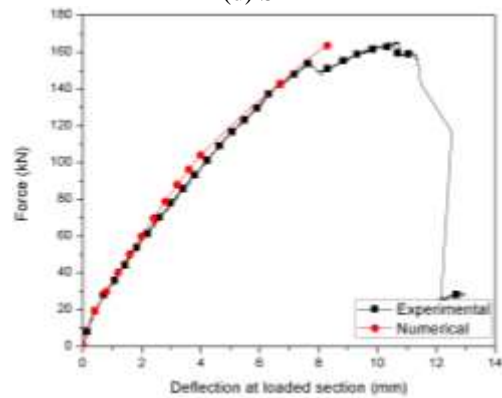
(f) SP-3L45

Figure 14. Comparison between experimental and numerical relationships of force vs. deflection at the loaded section

F =79 kN

0S-R

F =190.4 kN

7S-R

F =139 kN

NSM-4L90

F =118 kN
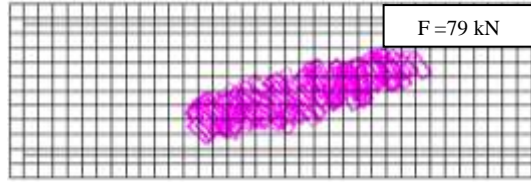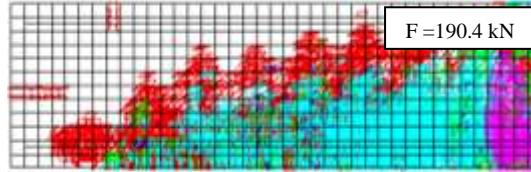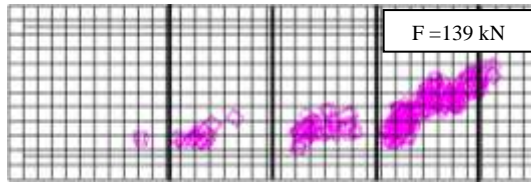
SP (concrete substrate)

SP (SHCC plate)

F =149 kN

SP-4L90 (concrete substrate)

SP-4L90 (HCP)

F =164 kN
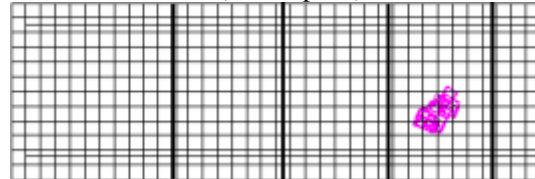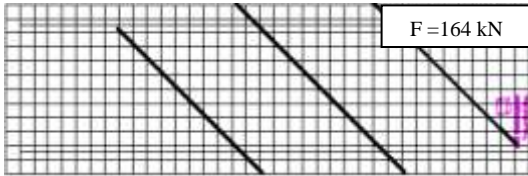
SP-3L45 (concrete substrate)
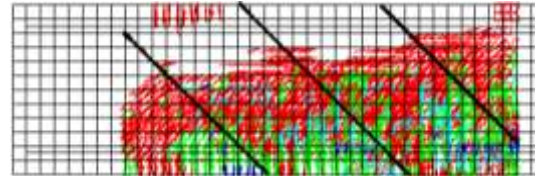
SP-3L45 (HCP)
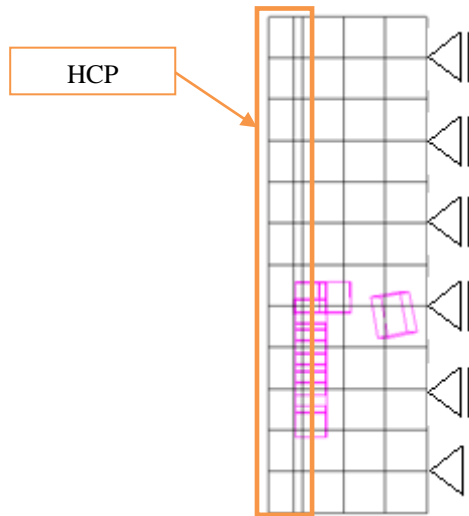
SP-3L45 (section B-B in Figure 12)

1   **Figure 15.** Crack pattern of the beams (pink color: crack completely open; red color: crack in the opening process;
2   cyan color: crack in the reopening process; green color: crack in the closing process; blue color: closed crack)
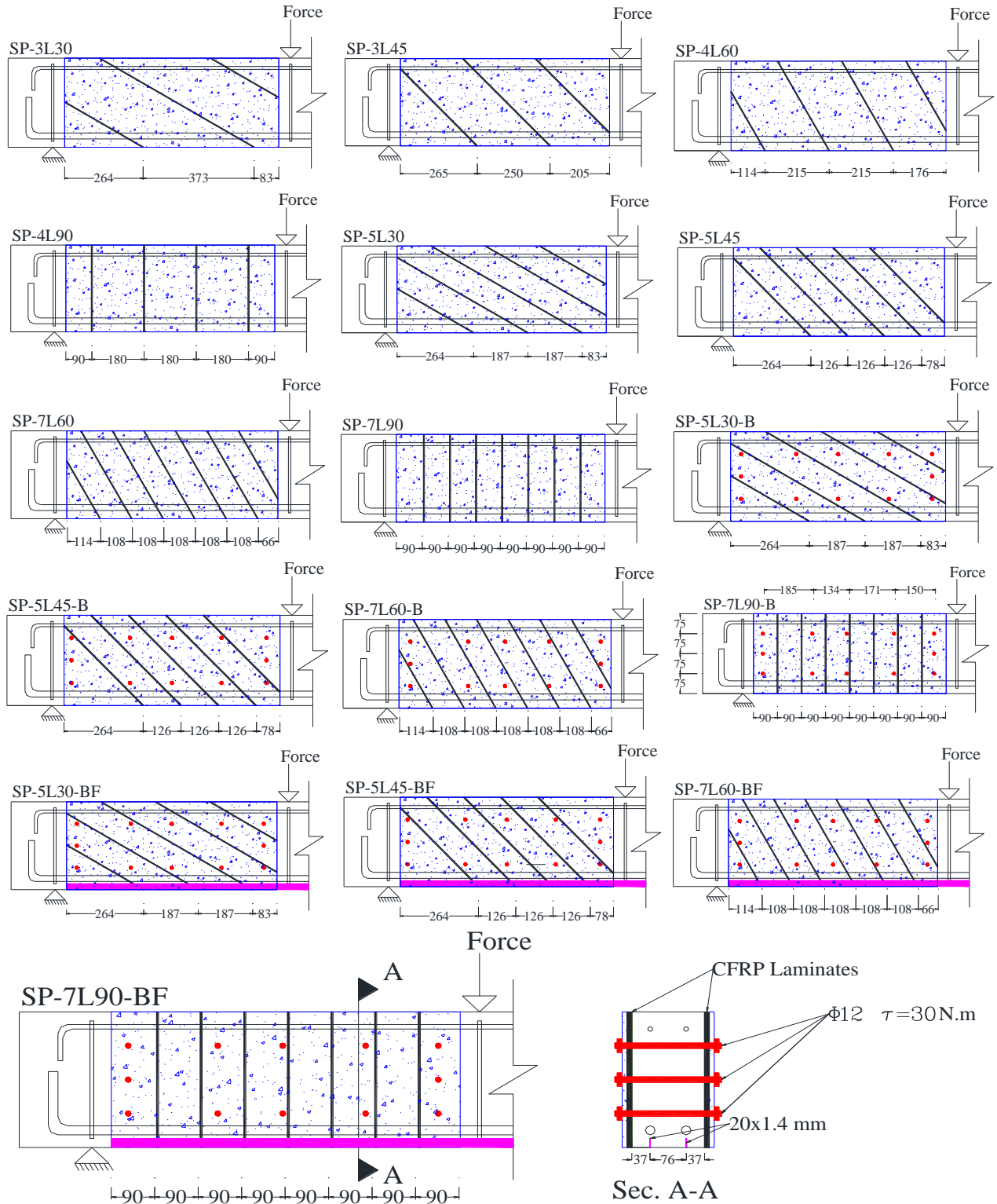
Figure 16. Strengthening scheme of the specimens (dimensions in mm)

SP-3L30 and SP-5L30

SP-3L45 and SP-5L45

SP-4L60 and SP-7L60
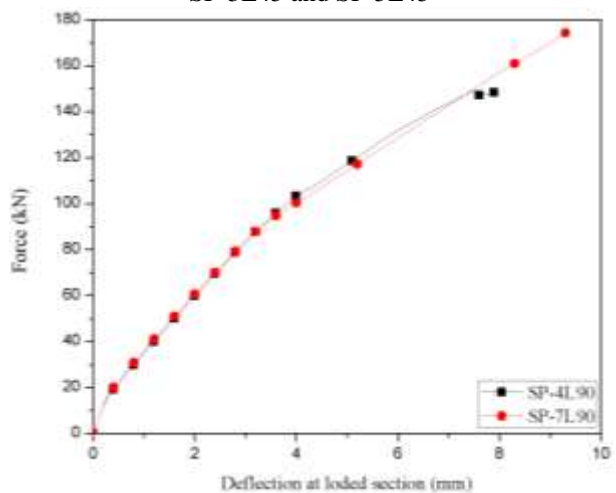
SP-4L90 and SP-7L90

1   **Figure 17.** Influence of inclination and percentage of the CFRP laminates on the relationship between the force and
2   the deflection at loaded section
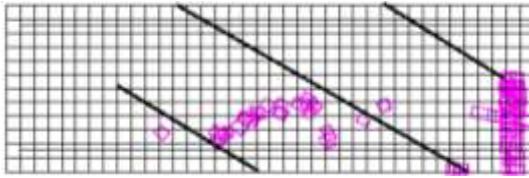
SP-3L30 (concrete substrate)
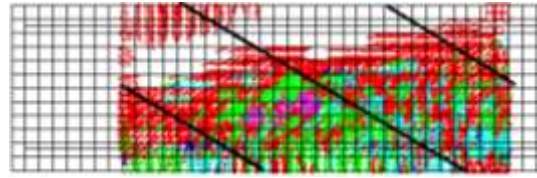
SP-3L30 (HCP)
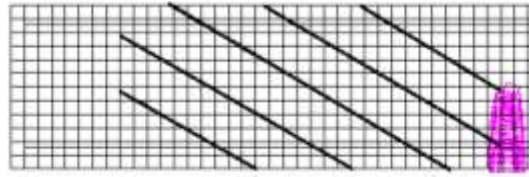
SP-5L30 (concrete substrate)
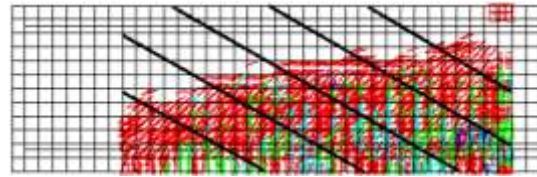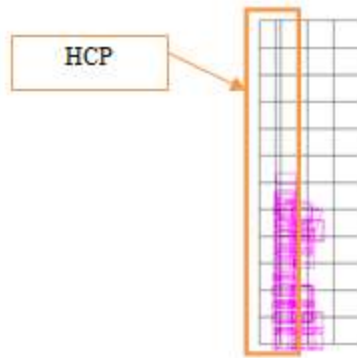
SP-5L30 (HCP)

Detachment of HCP in SP-5L30 beam
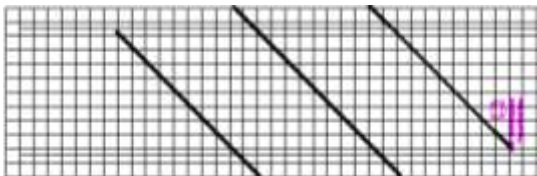
SP-3L45 (concrete substrate)
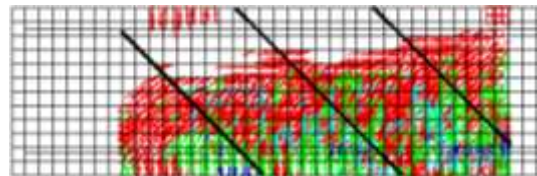
SP-3L45(HCP)
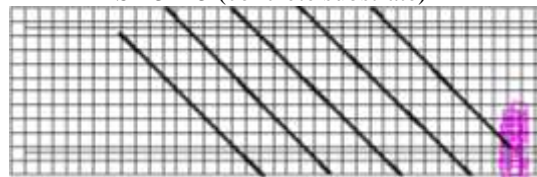
SP-5L45 (concrete substrate)
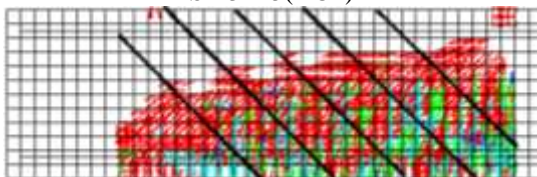
SP-5L45 (HCP)
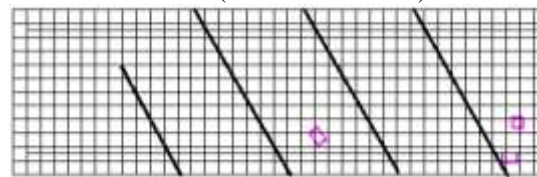
SP-4L60 (concrete substrate)
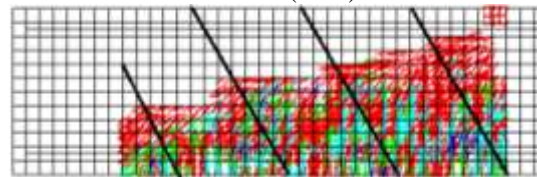
SP-4L60 (HCP)
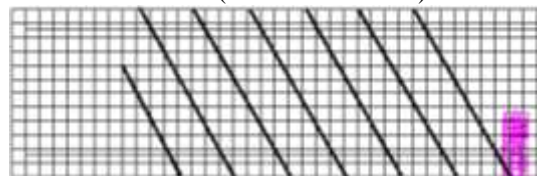
SP-7L60 (concrete substrate)
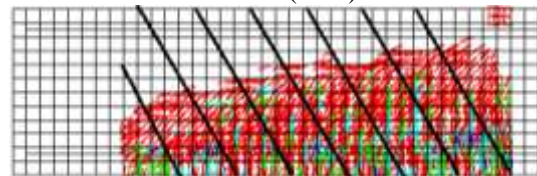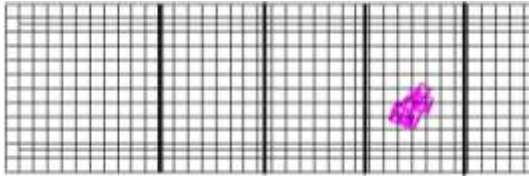
SP-7L60 (HCP)
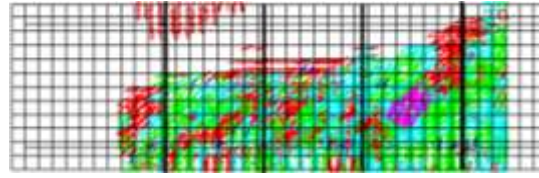
SP-4L90 (concrete substrate) SP-4L90 (HCP)
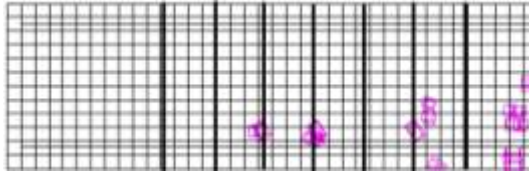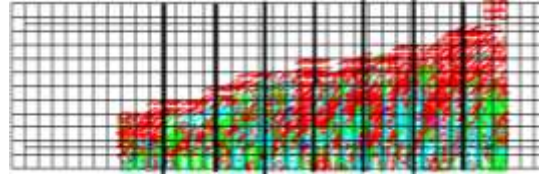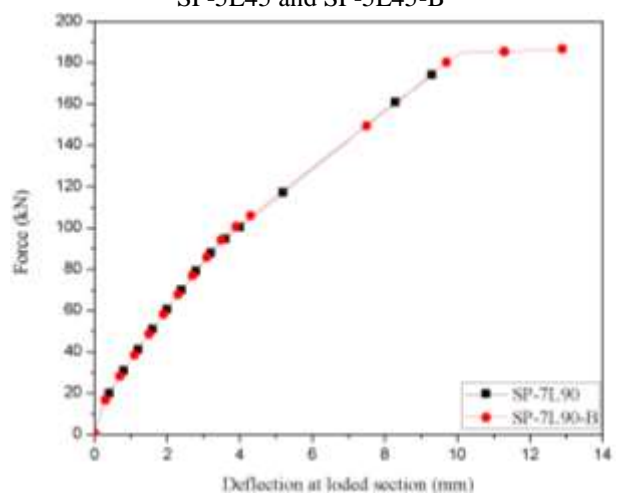
SP-7L90 (concrete substrate) SP-7L90 (HCP)

1   **Figure 18.** Influence of inclination and percentage of the CFRP laminates on the crack patterns
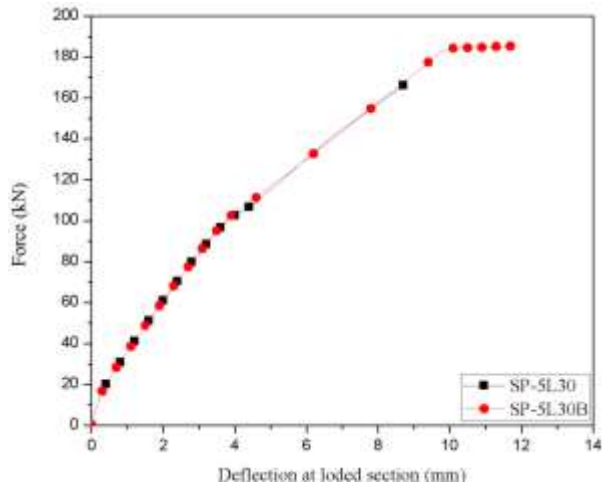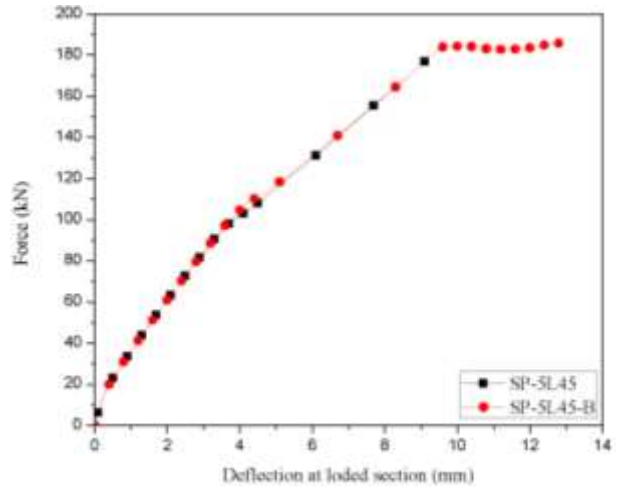
SP-5L30 and SP-5L30-B   SP-5L45 and SP-5L45-B
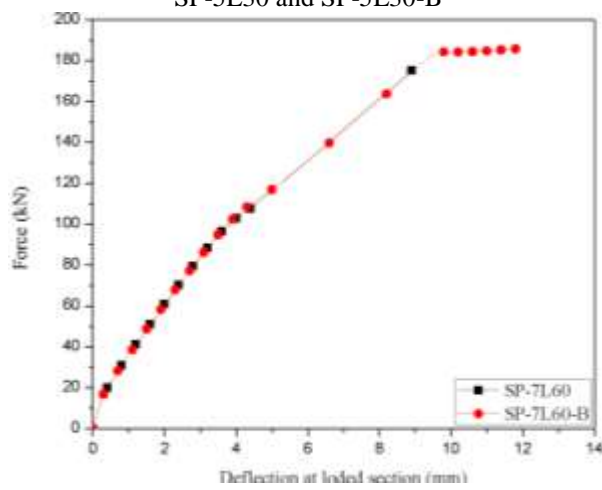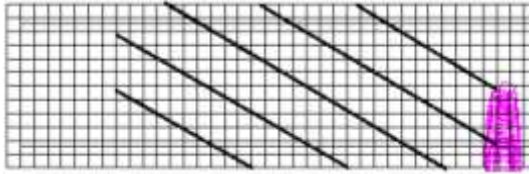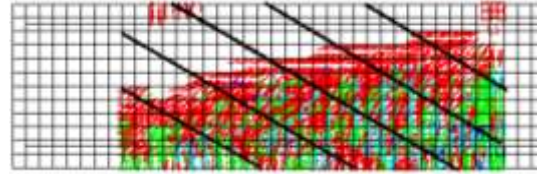
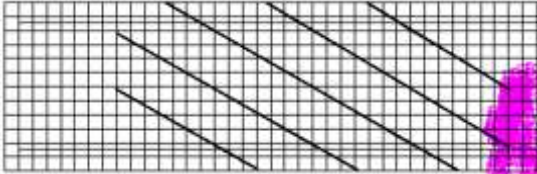SP-7L60 and SP-7L60-B   SP-7L90 and SP-7L90-B

1   **Figure 19.** Influence of through bolts on the relationship between the force and the deflection at loaded section
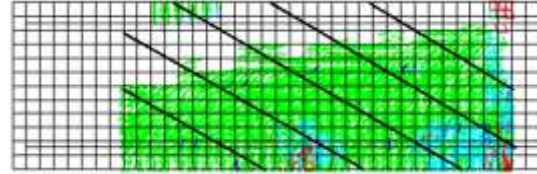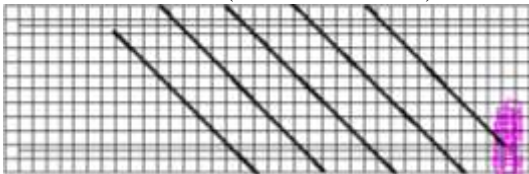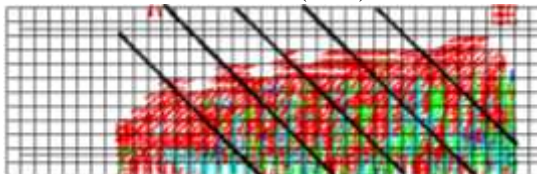
SP-5L30 (concrete substrate)

SP-5L30 (HCP)

SP-5L30-B (concrete substrate)
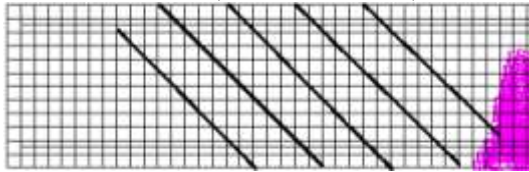

SP-5L30-B(HCP)

SP-5L45 (concrete substrate)

SP-5L45(HCP)

SP-5L45-B (concrete substrate)

SP-5L45-B (HCP)

SP-7L60 (concrete substrate)

SP-7L60 (HCP)

Detachment of HCP in SP-7L60 beam

SP-7L60-B (concrete substrate)

SP-7L60-B (HCP)

Flexural failure in SP-7L60-B beam

SP-7L90 (concrete substrate)

SP-7L90 (HCP)

SP-7L90-B (concrete substrate)
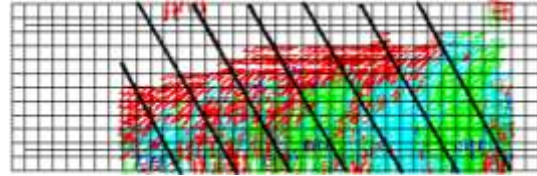
SP-7L90-B (HCP)
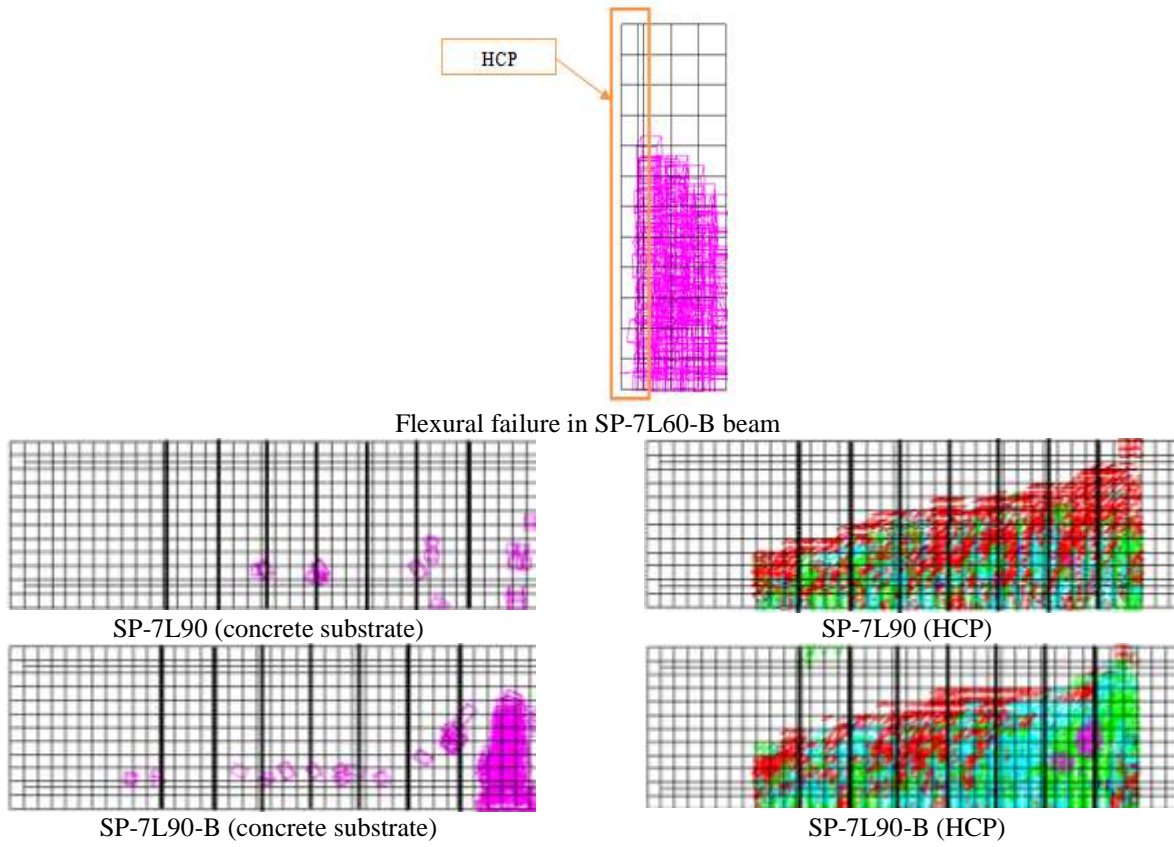
1   **Figure 20.** Influence of mechanical anchors on the failure of the beams
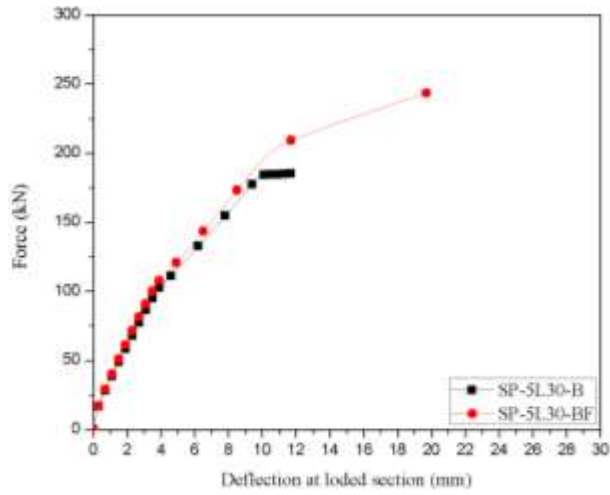
SP-5L30-B and SP-5L30-BF
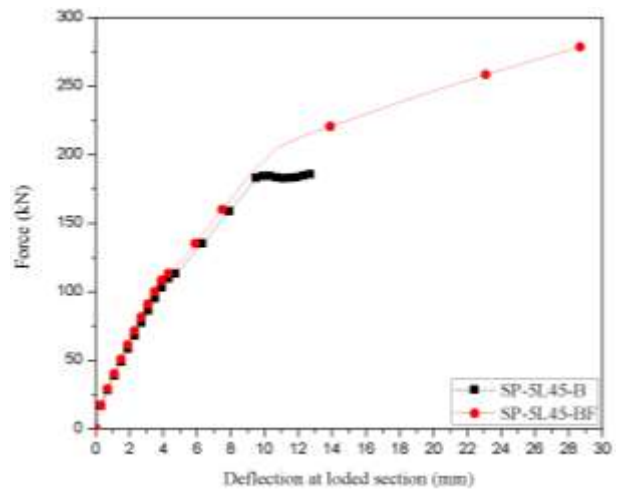
SP-5L45-B and SP-5L45-BF
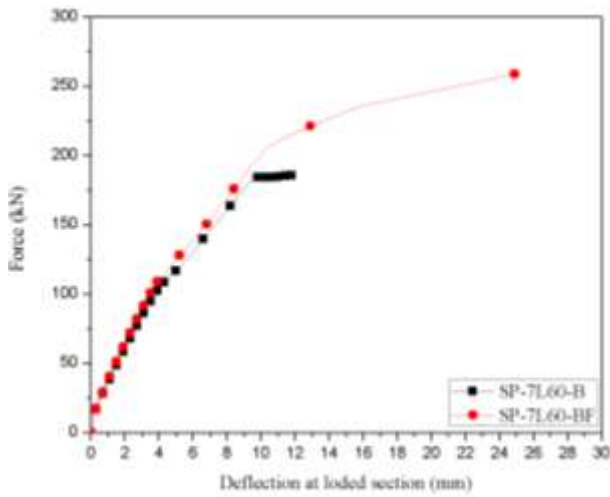
SP-7L60-B and SP-7L60-BF
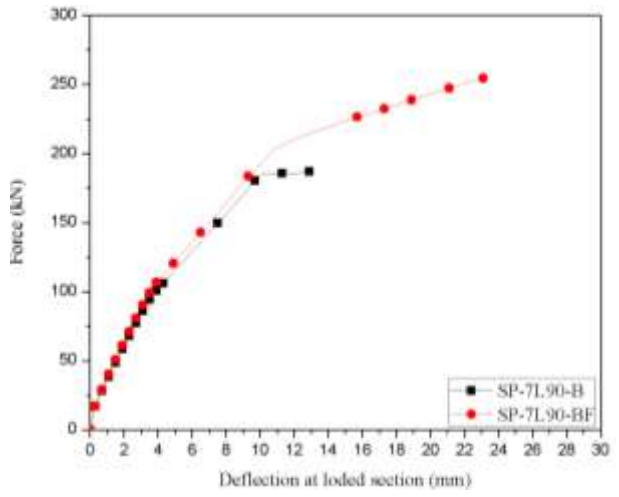
SP-7L90-B and SP-7L90-BF

1   **Figure 21.** Influence of Shear and Flexural strengthening of the RC beams on the relationship between load and
2   deflection

SP-5L30-B (concrete substrate)

SP-5L30-B (HCP)

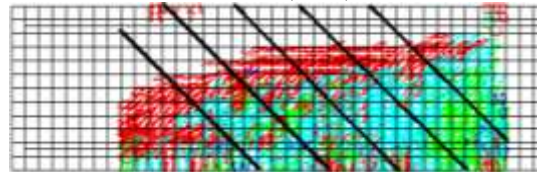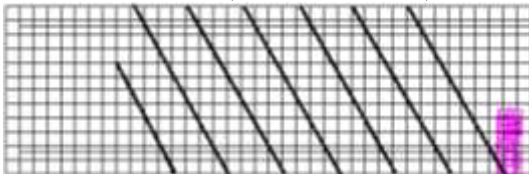SP-5L30BF (concrete substrate)

SP-5L30-BF (HCP)

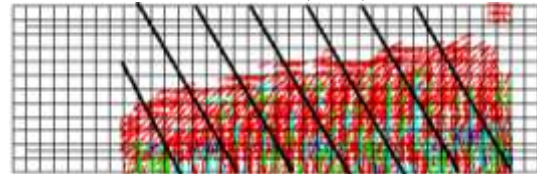SP-5L45-B (concrete substrate)
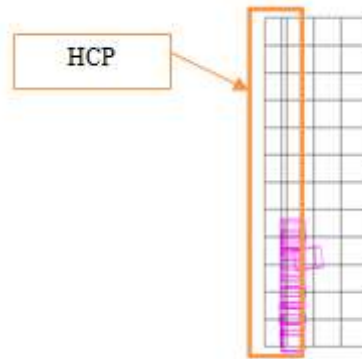
SP-5L45-B (HCP)
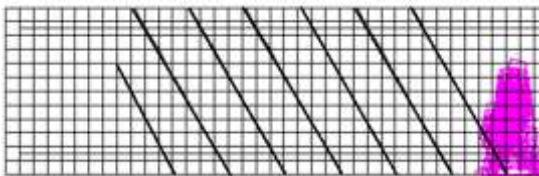
SP-5L45-BF (concrete substrate)

SP-5L45-BF (HCP)

SP-7L60-B (concrete substrate)

SP-7L60-B (HCP)

SP-7L60-BF (concrete substrate)

SP-7L60-BF (HCP)

SP-7L90-B (concrete substrate)

SP-7L90-B (HCP)

SP-7L90-BF (concrete substrate)

SP-7L90-BF (HCP)
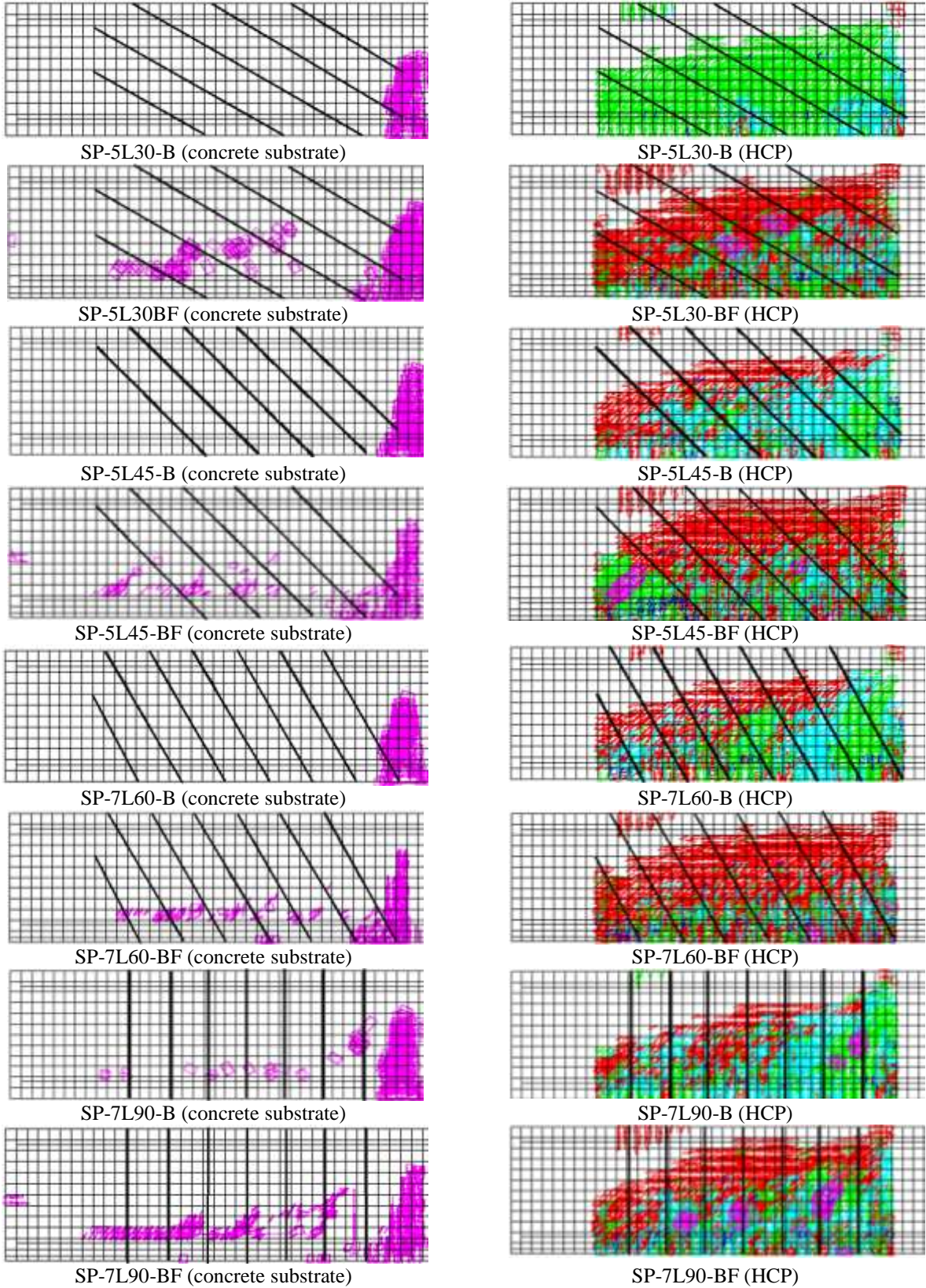
1   **Figure 22.** Influence of Shear and Flexural strengthening of the RC beams on the crack patterns

47

1 **LIST OF TABLE CAPTIONS**

2

3 **Table 1.** Shear strengthening/reinforcement configurations applied in the L_i beam's shear span of the tested beams

4 **Table 2.** SHCC mix procedure (Esmaeeli *et al.* 2013b)

5 **Table 3.** SHCC mix proportions based on the weight ratio percentage (Esmaeeli *et al.* 2013b)

6 **Table 4.** Values of the properties of intervening materials

7 **Table 5.** Relevant results in terms of load and deflection capacity

8 **Table 6.** Values of the parameters of the constitutive model for the concrete

9 **Table 7.** Values of the parameters of the constitutive model for the SHCC

10 **Table 8.** Values of the parameters of the steel constitutive model

Table 1. Shear strengthening/reinforcement configurations applied in the L_i beam's shear span of the tested beams

Beam designation	Shear strengthening/reinforcement configuration	Quantity	Percentage of CFRP laminates [1] (%)	Spacing, s_f, (mm)	Angle of CFRP laminates, θ_f, (°)
0S-R	-	-	-	-	-
NSM-4L90	NSM CFRP laminates of 1.4×10 mm² cross section	2×4 CFRP laminates	0.10	180	90
SP	SHCC Plates	20 mm thickness of SHCC	-	-	-
SP-4L90	HCPs (20 mm thickness of SHCC reinforced with CFRP laminates of 1.4×10 mm² cross section)	2×4 CFRP laminates	0.10	180	90
SP-3L45		2×3 laminates		250	45
7S-R	Steel stirrups	ϕ8	-	100	-

[1] $\rho_{fw} = \dfrac{2a_f b_f}{b_w s_f \sin\theta_f}$

1

Table 2. SHCC mix procedure (Esmaeeli *et al.* 2013b)

Step	Mix ingredients in each step	Duration (s)
1	S+C+FA	30
2	0.25W+SP	150
3	0.75W+VMA	150
4	Fibers	300

1   **Table 3.** SHCC mix proportions based on the weight ratio percentage (Esmaeeli *et al.* 2013b)

Fly ash/Cement	Water/B*	Sand / B*	Admixtures/B*	PVA fibers**
120	30	50	2.2	2

*B: Binder (cement + fly ash)

**Percentage of total composite mix volume.

Table 4. Values of the properties of intervening materials

Concrete	Compressive strength			
	f_{cm} =24.5 MPa (at 28 days)		f_{cm} =32.7 MPa (at 99 days)	
Steel	Tensile strength	$\phi 8$	$\phi 10$	$\phi 20$
	f_{sym} (yield stress)	544 MPa	529 MPa	576 MPa
	f_{sum} (tensile strength)	610 MPa	625 MPa	640 MPa
CFRP laminate	Tensile strength	Elasticity modulus		Maximum strain
	f_{fum} =2617 MPa	E_{fm} =149 GPa		ε_{fu} =1.6%
Epoxy adhesive	Tensile strength	Elasticity modulus		Maximum strain
	f_{fum} =18MPa	E_{fm} =6.8 GPa		ε_{fu} =0.4%
SHCC	Tensile stress at crack initiation	Tensile strength	Compressive strength	Young's modulus
	2.7 MPa	3.5MPa	31.6 MPa	18.4 GPa

1

Table 5. Relevant results in terms of load and deflection capacity

Beam designation	F_{max} (kN)	Deflection at loaded section (mm)	Shear resistance (kN) [1]	$(\frac{\Delta F}{F^{NSM-4L45}})_{max}$ (%)	$\frac{\Delta F_{max}}{F^{0S-R}_{max}}$ (%)	$\frac{F_{max}}{F^{7S-R}_{max}}$ (%)
0S-R	81	3.3	51	-	-	44
NSM-4L90	143	8.2	91	0	77	79
SP	130	6.3	82	4	60	71
SP-4L90	151	8.3	96	14	87	83
SP-3L45	166	12.5	106	39	105	91
7S-R	182	19.9	116	37	125	100

2

[1] $P = \dfrac{L_r}{L_i + L_r}$

1

Table 6. Values of the parameters of the constitutive model for the concrete

Poisson's ratio (ν_c)	0.19
Initial Young's modulus (E_c)	$31381 \ N/mm^2$
Compressive strength (f_c)	$32.7 \ N/mm^2$
Tri-linear tension-stiffening diagram	$f_{ct} = 2.0 \ N/mm^2$; $G_f = 0.07 \ N/mm$ $\xi_1 = 0.007$; $\alpha_1 = 0.3$; $\xi_2 = 0.1$; $\alpha_2 = 0.3$
Parameter defining the mode I fracture energy available for the new crack	$n = 3$
Parameters for defining the softening crack shear stress-shear strain diagram of concrete in the tension-stiffening	$\tau_{t,p}^{cr} = 1.0 \ N/mm^2$; $G_{f,s} = 0.02 \ N/mm$ $\beta = 0.6$
Crack bandwidth, l_b	*Cube root of the volume associated with the integration point*
Threshold angle	$\alpha_{th} = 30^o$
Maximum number of cracks per integration point	2

1   **Table 7.** Values of the parameters of the constitutive model for the SHCC

Poisson's ratio (v_c)	0.15
Initial Young's modulus (E_c)	18420 N/mm^2
Compressive strength (f_c)	31.60 N/mm^2
Tri-linear tension-stiffening diagram	$f_{ct} = 2.7\,N/mm^2$; $G_f = 0.46\,N/mm$ $\xi_1 = 0.98$; $\alpha_1 = 1.16$; $\xi_2 = 0.99$; $\alpha_2 = 1.0$
Parameter defining the mode I fracture energy available for the new crack	$n = 3$
Parameters for defining the softening crack shear stress-shear strain diagram of concrete in the tension-stiffening	$\tau_{t,p}^{cr} = 1.0\,N/mm^2$; $G_{f,s} = 0.1\,N/mm$; $\beta = 0.4$
Crack bandwidth, lb	*Cube root of the volume associated with the integration point*
Threshold angle	$\alpha_{th} = 30^o$
Maximum number of cracks per integration point	2

1

Table 8. Values of the parameters of the steel constitutive model

Property	$\phi8$	$\phi10$	$\phi20$
f_{sym} (N/mm^2)	546	529	576
f_{sum} (N/mm^2)	610	625	640
ε_{sy} (‰)	2.4	2.5	2.6
σ_{sy} (N/mm^2)	546	529	576
ε_{sh} (‰)	35	30	35
σ_{sh} (N/mm^2)	558	529	579
ε_{su} (‰)	100	150	100
σ_{su} (N/mm^2)	610	625	640
Third branch exponent	1	1	1

2

3

4

5

6

7

8

9

10

11

12

13

14

15

16

17

18

19

20